BIOPHYSICS

A genetically encoded actuator boosts L-type calcium channel function in diverse physiological settings

Pedro J. del Rivero Morfin[1], Diego Scala Chavez[2], Srinidhi Jayaraman[1], Lin Yang[3], Stefanie M. Geisler[4], Audrey L. Kochiss[1], Petronel Tuluc[4], Henry M. Colecraft[1,5], Steven O. Marx[3,5], X. Shawn Liu[1,6], Anjali M. Rajadhyaksha[2,7,8], Manu Ben-Johny[1]*

L-type Ca^{2+} channels ($Ca_V1.2/1.3$) convey influx of calcium ions that orchestrate a bevy of biological responses including muscle contraction, neuronal function, and gene transcription. Deficits in Ca_V1 function play a vital role in cardiac and neurodevelopmental disorders. Here, we develop a genetically encoded enhancer of $Ca_V1.2/1.3$ channels ($GeeC_L$) to manipulate Ca^{2+} entry in distinct physiological settings. We functionalized a nanobody that targets the Ca_V complex by attaching a minimal effector domain from an endogenous Ca_V modulator—leucine-rich repeat containing protein 10 (Lrrc10). In cardiomyocytes, $GeeC_L$ selectively increased L-type current amplitude. In neurons in vitro and in vivo, $GeeC_L$ augmented excitation-transcription (E-T) coupling. In all, $GeeC_L$ represents a powerful strategy to boost $Ca_V1.2/1.3$ function and lays the groundwork to illuminate insights on neuronal and cardiac physiology and disease.

INTRODUCTION

L-type calcium (Ca^{2+}) channels ($Ca_V1.2$ and $Ca_V1.3$) are biologically crucial as they convert electrical signals to Ca^{2+} influx that orchestrates a vast array of physiological processes (*1*–*3*). These include: (i) shaping the action potential (AP) and initiating excitation-contraction (E-C) coupling in the heart (*4*), (ii) tuning neuronal excitability (*5*, *6*) and excitation-transcription (E-T) coupling that contributes to synaptic plasticity (*7*–*10*) in neurons, (iii) enabling insulin secretion in pancreatic beta cells (*11*), (iv) regulating AP firing and catecholamine release from adrenal chromaffin cells (*12*), (v) supporting smooth muscle contraction (*13*), (vi) triggering vesicle secretion in inner ear hair cells (*14*), and (vii) varying functions in nonexcitable cells (*15*). From a pathophysiological perspective, gain-of-function $Ca_V1.2$ variants are linked to a multisystem disorder, Timothy syndrome (*16*), while loss-of-function variants are associated with cardiac arrhythmias (*17*, *18*) and variable neurological phenotypes (*17*, *19*). Beyond this, $Ca_V1.2$ (*CACNA1C*) and/or $Ca_V1.3$ (*CACNA1D*) channels have been found to be prominent risk genes for various neurodevelopmental and neuropsychiatric disorders [see reviews (*20*, *21*)] including autism spectrum disorders (ASDs) (*16*), schizophrenia (*22*, *23*), and bipolar disorder (*24*), suggesting important yet complex functions in the brain. The emerging consensus is that either up-regulation or down-regulation of channel function can contribute to human disease, likely depending on the specific cell type or neural circuit involved (*20*). However, our current understanding of the physiology of these channels and their pathophysiological consequences are derived largely from either constitutive or cell type–specific knockout of $Ca_V1.2$ and/or $Ca_V1.3$ in mice (*3*, *25*). By comparison, there are limited strategies available for targeted up-regulation of $Ca_V1.2/1.3$ function. This limitation hampers an in-depth understanding of the biological mechanisms.

From an experimental perspective, development of next-generation customizable Ca_V1 actuators is highly desirable to illuminate complex physiology. Pharmacologically, Ca_V1 blockers including dihydropyridines and phenylalkylamines are used clinically for various indications, e.g., hypertension, migraine, and arrhythmias (*2*, *26*). Genetically encoded inhibitors of Ca_V channels have also been engineered by leveraging channel modulation by Rem/Gem/Kir family of G proteins (*27*) or by targeted ubiquitination of channel complexes (*28*). Conversely, activation of Ca_V1 channels is a double-edged sword—non-tissue–specific pharmacological Ca_V1 agonists can be deleterious. Administration of Ca_V1 agonists Bay K 8644 and FPL 64176 result in severe motor abnormalities (*29*), seizures (*30*), and self-harming behavior (*31*) in rodents. Thus, alternate strategies for targeted or tissue specific up-regulation of Ca_V1 function are necessary (*32*).

Here, we sought to develop a molecular actuator of $Ca_V1.2/Ca_V1.3$ that up-regulates channel activity in distinct physiological settings. Beyond the pore-forming subunit that is targeted by conventional pharmacology (*33*), Ca_V channels associate with a bevy of regulatory proteins (*34*) that fine-tune channel dynamics (*2*, *35*). We reasoned that leveraging an intracellular regulatory protein may provide an alternative strategy to engineer a genetically encodable Ca_V enhancer. Accordingly, we used a recently identified $Ca_V1.2$ modulator—leucine-rich repeat containing protein 10 (Lrrc10)—that enhances $Ca_V1.2$ current in heterologous systems and ventricular cardiomyocytes (*36*). Lrrc10 exhibits cardiac-specific expression and has been implicated in cardiomyocyte maturation (*37*, *38*), regeneration (*39*–*41*), and response to increased afterload (*42*). We identified a minimal effector domain within Lrrc10 that up-regulates $Ca_V1.2$, albeit with a low affinity such that it poorly modulates channel function by itself. Instead, fusion of this domain to a nanobody that binds the Ca_V complex with a high affinity yielded a $Ca_V1.2/1.3$ specific actuator, termed genetically encoded enhancer of Ca^{2+} channels—L-type ($GeeC_L$), that markedly increases the channel open probability (P_O). We deployed $GeeC_L$ into cardiomyocytes and

[1]Department of Physiology and Cellular Biophysics, Columbia University, New York, NY, USA. [2]Pediatric Neurology, Department of Pediatrics, Weill Cornell Medicine, New York, NY, USA. [3]Division of Cardiology, Department of Medicine, Columbia University, Vagelos College of Physicians and Surgeons, New York, NY, USA. [4]Department of Pharmacology and Toxicology, University of Innsbruck, Innsbruck, Tyrol, Austria. [5]Department of Molecular Pharmacology and Therapeutics, Columbia University, New York, NY, USA. [6]Herbert Irving Comprehensive Cancer Center, Columbia University Medical Center, New York, NY, USA. [7]Feil Family Brain and Mind Research Institute, Weill Cornell Medicine, New York, NY, USA. [8]Weill Cornell Autism Research Program, Weill Cornell Medicine, New York, NY, USA.
*Corresponding author. Email: mbj2124@cumc.columbia.edu

neurons to modulate endogenous $Ca_V1.2$/$Ca_V1.3$ currents and to tune downstream physiological functions.

RESULTS

A $Ca_V1.2$ actuator was engineered by leveraging Lrrc10 modulation

To establish its potential utility as a Ca_V enhancer, we sought to corroborate Lrrc10 association with full-length $Ca_V1.2$ channels using a live-cell flow cytometry–based fluorescence resonance energy transfer (FRET) 2-hybrid assay. We tagged Lrrc10 with a cerulean fluorescent protein and $Ca_V1.2$ α-subunit with a venus fluorescent protein. We found robust FRET between holo-$Ca_V1.2$ and full-length Lrrc10 (Fig. 1A). To quantify the functional consequences of Lrrc10 interaction, we undertook whole-cell recordings of $Ca_V1.2$, cotransfected with auxiliary subunits $\alpha_2\delta_1$ and β_{2b} in human embryonic kidney (HEK) 293 cells and measured changes in peak current density (J_{peak}). When compared to cells expressing only $Ca_V1.2$ canonical subunits, coexpression of Lrrc10 yielded a marked increase in J_{peak} (Fig. 1, B and C). Further quantification of normalized tail current amplitudes revealed an ~8-mV hyperpolarizing shift in $V_{1/2}$ of activation in the presence of Lrrc10 (fig. S1A-B, G), consistent with previous reports (*36*).

Similar to other Lrr containing proteins, Lrrc10 is composed of seven Lrr domains with signature sequences LxxLxLxxNxL or LxxLxLxxNxxL flanked by short N-terminal (NT) and C-terminal (CT)

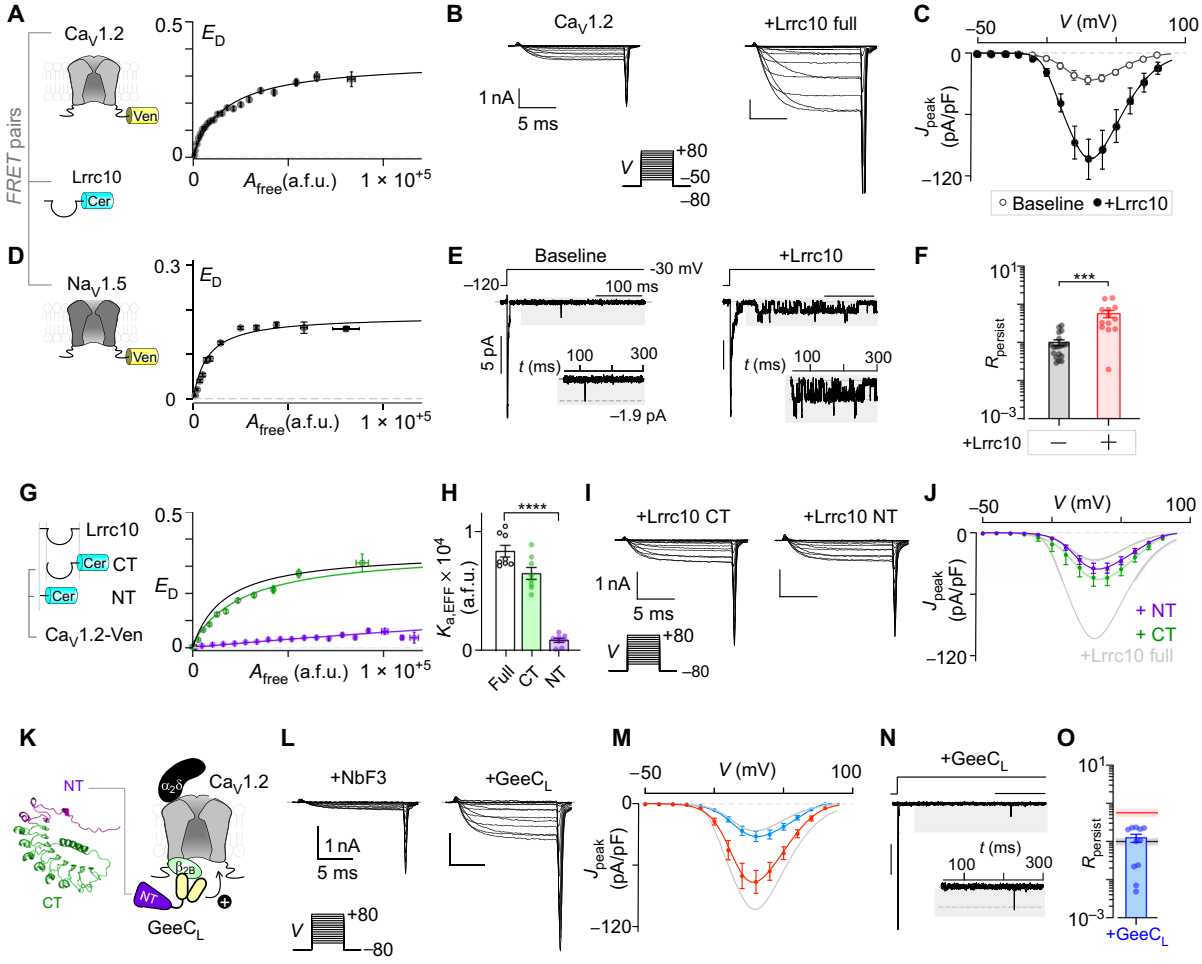

Fig. 1. Leveraging Lrrc10 modulation of $Ca_V1.2$ to develop a genetically encoded enhancer. (**A**) Flow cytometric FRET 2-hybrid assay shows robust $Ca_V1.2$ binding to Lrrc10. [$K_{a,EFF} = 8.3 \times 10^{-5} \pm 4.8 \times 10^{-5}$ arbitrary fluorescence units (a.f.u.), $n = 8$]. Left: Schematic. Right: Binned data of FRET efficiency (E_D) versus free acceptor concentration (A_{free}). Each dot represents means ± SEM. (**B**) Exemplar traces show $Ca_V1.2$ without (left) or with Lrrc10 (right) evoked by 15-ms test pulses from −50 to +80 mV in 10-mV intervals. (**C**) Lrrc10 up-regulates peak $Ca_V1.2$ current density (J_{peak}). Each dot represents mean ± SEM. $n = 8$ (baseline) and 15 cells (+Lrrc10) from three transfections. (**D**) FRET analysis confirms interaction of $Na_V1.5$ with Lrrc10. ($K_{a,EFF} = 1.4 \times 10^{-4} \pm 1.8 \times 10^{-5}$, $n = 4$). (**E**) Exemplar multichannel recordings of $Na_V1.5$ with (right) or without Lrrc10 (left). (**F**) Bar graph summary of I_{NaL} measured as $R_{persist}$. Each bar, means ± SEM. $n = 19$ (no Lrrc) and 13 cells (+Lrrc10) from three transfections. (**G**) FRET analysis shows differential binding of Lrrc10 NT and CT with $Ca_V1.2$. Format as in (A). (**H**) Bar graph summary of $K_{a,EFF}$ for $Ca_V1.2$ association Lrrc10 fragments. ****$P < 0.0001$ by one-way analysis of variance (ANOVA) followed by Tukey's test. (**I**) Both Lrrc10 CT (left) and NT (right) fail to up-regulate $Ca_V1.2$. (**J**) Population J_{peak}-V relationship confirms minimal changes in $Ca_V1.2$ with Lrrc10 NT or CT. $n = 9$ (CT) and 27 cells (NT) from three transfections. (**K**) Schematic shows AlphaFold3-predicted structure of Lrrc10 and design of GeeC$_L$. (**L**) GeeC$_L$ (right) but not nbF3 (left) enhances $Ca_V1.2$. (**M**) Population data confirms a robust increase in J_{Peak} of $Ca_V1.2$ with GeeC$_L$ compared to Nb.F3 alone. $n = 14$ cells each from three transfections. (**N**) Exemplar multichannel recordings of $Na_V1.5$ show low I_{NaL} with GeeC$_L$. (**O**) Bar graph shows minimal increase in I_{NaL} with GeeC$_L$. Blue bar, means ± SEM. Black, $Na_V1.5$; red, Lrrc10 from (F).

regions (*43*). Traditionally, the Lrr domains are thought to support protein-protein interactions, allowing this diverse family of proteins to interact with a wide range of proteins to tune cellular functions (*44*). Hence, we reasoned that Lrrc10 may interact with related ion channels and possibly modulate their function. To test this possibility, we undertook FRET 2 hybrid analysis probing Lrrc10 association with $Na_V1.5$ channels, which share structural homology with $Ca_V1.2$. The coexpression of Cerulean-tagged Lrrc10 with Venus-tagged $Na_V1.5$ revealed a Langmuir binding isotherm (Fig. 1D). To determine the functional consequence of Lrrc10 interaction with $Na_V1.5$, we undertook multichannel recordings to measure changes in late Na current (I_{NaL}), a key vulnerability that increases the risk for cardiac arrhythmias. At baseline, $Na_V1.5$ activates and inactivates rapidly, resulting in minimal channel openings during prolonged depolarization (Fig. 1, E and F), consistent with minimal baseline I_{NaL} (Fig. 1F). Here, I_{NaL} is quantified as $R_{persist}$, the ratio of average P_O following 50 ms of depolarization to the peak P_O. In the presence of Lrrc10, we observed an ~5-fold increase in I_{NaL} (Fig. 1, E and F). These findings suggest that simply overexpressing Lrrc10 as a strategy to boost $Ca_V1.2$ may be detrimental.

Accordingly, we sought to engineer Lrrc10 to preferentially target Ca_V1 channels. To do so, we sought to identify key segments within Lrrc10 responsible for binding and modulating Ca_V channels. We used a flow cytometry–based FRET 2-hybrid assay to probe interaction of Lrrc10 segments with holo-$Ca_V1.2$ in live cells (Fig. 1G). Specifically, we bisected Lrrc10 into (i) an NT domain and (ii) a CT segment that included the Lrr domains. We found that the Lrrc10 CT segment revealed strong binding to $Ca_V1.2$ with a relative association constant ($K_{a,EFF}$) that is similar to full-length Lrrc10 (Fig. 1, G and H). By comparison, the isolated Lrrc10 NT domain showed weak to no binding (Fig. 1, G and H). These results suggest that the Lrrc10 CT containing the Lrr domains is critical for robust $Ca_V1.2$ interaction. Thus affirmed, we probed whether Lrrc10 CT also sufficed for functional modulation of $Ca_V1.2$. Unexpectedly, we found that coexpression of Lrrc10 CT only minimally changed J_{peak} despite its ability to interact with full-length $Ca_V1.2$ (Fig. 1, I and J). Furthermore, coexpression of the Lrrc10 NT domain also revealed little to no change in J_{peak}, likely reflecting its weak affinity for $Ca_V1.2$ (Fig. 1, I and J). The analysis of normalized tail current measurements showed a ~8 mV-depolarizing shift in voltage dependence of activation (V_h) with Lrrc10 CT but no change with Lrrc10 NT (fig. S1, C and D and G). Together, these results point to two distinct possibilities: (i) the overall tertiary structure of Lrrc10 may be essential for functional $Ca_V1.2$ modulation, such that any alteration in its structure abrogates its function, or (ii) Lrrc10 may be composed of two functionally distinct domains: The CT segment containing the Lrr domains may be responsible for high-affinity binding to $Ca_V1.2$, while the NT segment may be a low-affinity effector domain responsible for driving Ca^{2+} current up-regulation.

We reasoned that if Lrrc10 CT serves as a binding domain for $Ca_V1.2$, then replacing this region with a peptide or a domain that interacts with $Ca_V1.2$ while preserving Lrrc10 NT would maintain functional modulation. In this regard, recent studies have reported a nanobody Nb.F3 that binds to the $Ca_V\beta$ subunit with a high affinity (~10 nM) but is functionally inert (*45*). Hence, we engineered a chimeric protein by fusing the Lrrc10 NT region with Nb.F3 and probed its effect on tuning $Ca_V1.2$ currents (Fig. 1K). Coexpression of Nb.F3 with $Ca_V1.2$ yielded no change in J_{peak}, consistent with the nanobody being functionally silent (Fig. 1, L and M). However, coexpression of the chimeric Lrrc10 NT fused to Nb.F3 resulted in a nearly threefold increase in J_{peak} (Fig. 1, L and M). However, this maneuver did not yield an appreciable change in voltage dependence of channel activation (fig. S1, E to H). Given its ability to up-regulate $Ca_V1.2$ currents, we named this chimeric protein "genetically encoded enhancer of Ca^{2+} currents—L-type" or $GeeC_L$. Unlike full-length Lrrc10, coexpression of $GeeC_L$ with $Na_V1.5$ resulted in minimal changes in I_{NaL} compared to baseline conditions (Fig. 1, N and O). Overall, one possible explanation is that Lrrc10 has a bimodular architecture, whereby the NT serves as a low-affinity effector domain to increase currents, while the CT serves as a binding domain that supports association with $Ca_V1.2$. It is also possible that truncating Lrrc10 alters its fold and diminishes its function. Notably, as Lrr repeats often interact promiscuously with protein targets, this chimeric approach provides a potential platform for targeted up-regulation of Ca_V channels in distinct physiological settings, avoiding detrimental off-target effects.

$GeeC_L$ selectively up-regulates $Ca_V1.2/1.3$ channels

Having confirmed the ability of $GeeC_L$ to enhance $Ca_V1.2$ currents, we sought to determine the selectivity of $GeeC_L$ in tuning various members of the Ca_V channel superfamily. All members of the Ca_V1/Ca_V2 family are known to interact with the $Ca_V\beta$ subunit targeted by $GeeC_L$ (*46*). Hence, it is possible that any of these channels may be modulated by $GeeC_L$. By comparison, Ca_V3 channels do not require the $Ca_V\beta$ subunit for its function (*47*) and are unlikely to be affected by $GeeC_L$. Accordingly, we systematically quantified changes in J_{peak} of other Ca_V channels upon coexpression with $GeeC_L$. Similar to $Ca_V1.2$, we found that $GeeC_L$ yielded a marked increase in $Ca_V1.3$ currents compared to coexpression of Nb.F3 (Fig. 2, A and F). By contrast, the closely related $Ca_V1.4$ channels were entirely unaffected (Fig. 2, B and F). Furthermore, we found that $GeeC_L$ had minimal effect on Ca_V2 channels (Fig. 2, C to F). To determine whether this pattern of selectivity for $GeeC_L$ reflects that of wild-type Lrrc10, we coexpressed full-length Lrrc10 with $Ca_V1.3$ and $Ca_V2.1$. As expected, we found that Lrrc10 enhanced J_{peak} of $Ca_V1.3$ but not $Ca_V2.1$ (fig. S2). Together, these findings demonstrate that $GeeC_L$ is selective in up-regulating $Ca_V1.2/1.3$ channels.

$GeeC_L$ enhances $Ca_V1.2$ function by increasing P_O

Mechanistically, $GeeC_L$ may up-regulate $Ca_V1.2/1.3$ whole-cell current by enhancing one of three fundamental elementary channel properties: (i) the P_O, i.e., the likelihood that channel is open at any given voltage; (ii) the unitary current (i), which describes the current through a single open channel; or (iii) the total number of channels (N) at the surface membrane. To distinguish between these possibilities, we undertook low-noise, cell-attached, single-channel recordings of $Ca_V1.2$ coexpressed with $\alpha_2\delta_1$ and β_{2B} in HEK 293 cells (Fig. 3, A to D). These recordings permit direct measurement of both P_O and i while preserving the intracellular milieu. Here, we use Ba^{2+} as charge carrier to avoid the confounding effects of Ca^{2+}-dependent inactivation. Stochastic channel openings were evoked at near steady-state P_O at each voltage using a slow voltage ramp. Figure 3A shows elementary channel openings for $Ca_V1.2$ as downward deflections to the unitary current level at each voltage (gray slanted curve). Coexpression of $GeeC_L$ (Fig. 3B) but not nb.F3 (Fig. 3C) increased channel openings. The steady-state P_O-voltage relationship was estimated by averaging 80 to 150 stochastic records to obtain a mean current that is divided into the open level and averaged over

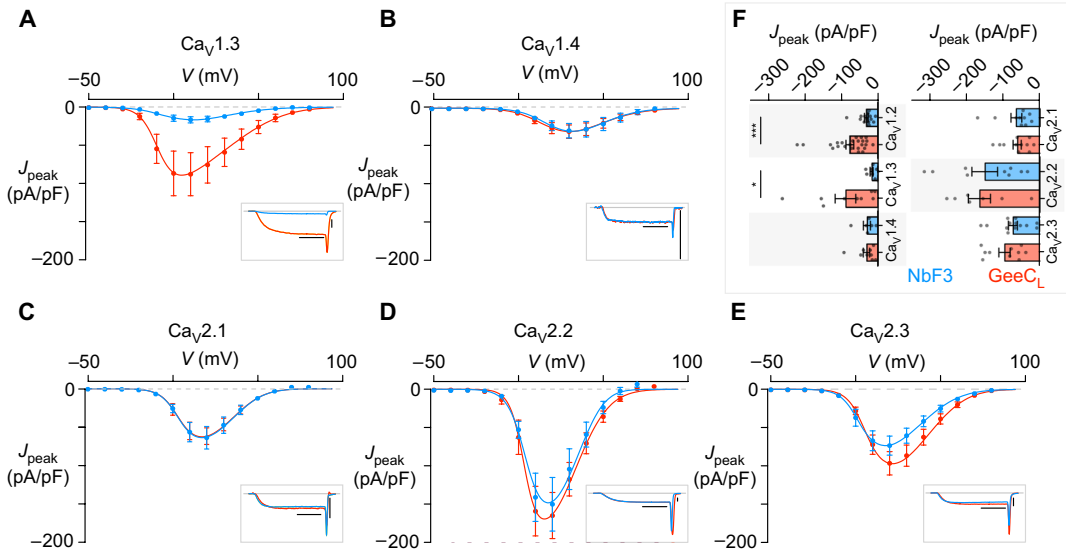

Fig. 2. $GeeC_L$ selectively enhances $Ca_V1.2/1.3$ currents. (**A**) Coexpression of $GeeC_L$ (red) increases $Ca_V1.3$ currents in HEK 293 cells compared to nb.F3 (blue). Inset shows exemplar recordings in the presence of nb.F3 or $GeeC_L$. Error bars show mean and SEM. (**B**) $GeeC_L$ minimally perturbs peak current density of $Ca_V1.4$ channels. Format as in (A). (**C** to **E**) $GeeC_L$ fails to alter peak current density of $Ca_V2.1$ (C), $Ca_V2.2$ (D), and $Ca_V2.3$ (E) channels. Format as in (A). (**F**) Bar graphs compare peak current density for various $Ca_V1/2$ channels in the presence of nb.F3 (blue) or $GeeC_L$ (red). Error bars show mean and SEM. Statistical analysis: Kolmogorov-Smirnov normality test followed by Mann-Whitney test ($Ca_V1.2$, $Ca_V1.3$, $Ca_V2.1$) and unpaired Student's *t* test ($Ca_V1.3$ $Ca_V2.2$, and $Ca_V2.3$). $*P < 0.05$ and $***P < 0.001$. $n = 14$ and 24 (−/+ $GeeC_L$, $Ca_V1.2$); $n = 7$ and 9 (−/+ $GeeC_L$, $Ca_V1.3$); $n = 6$ and 9 (−/+ $GeeC_L$, $Ca_V1.4$); $n = 10$ and 11 (−/+ $GeeC_L$, $Ca_V2.1$); $n = 9$ and 7 (−/+ $GeeC_L$, $Ca_V2.2$); and $n = 13$ and 10 (−/+ $GeeC_L$, $Ca_V2.3$) from two to three transfections.

multiple patches. We found that $GeeC_L$ increased the maximal P_O compared to control conditions or with nb.F3 alone (Fig. 3D and fig. S3A). No changes in V_h (fig. S3B) or slope factor (SF) were observed (fig. S3C).

To determine whether $GeeC_L$ alters surface-membrane trafficking of $Ca_V1.2$, we used a dual labeling approach (Fig. 3E) (*48*). Specifically, the pore-forming α subunit of $Ca_V1.2$ was engineered to contain tandem bungarotoxin (BTX) binding sites on a loop exposed to the extracellular surface and a yellow fluorescent protein (YFP) on its C terminus. With this assay, the total number of channels in single cells can be measured as the fluorescence intensity of YFP, while the surface-membrane channels can be selectively labeled by incubating cells with BTX conjugated to Alexa Fluor 647. We observed robust baseline surface expression for $Ca_V1.2$ when coexpressed with β_{2b} as reported by normalized Alexa Fluor 647 signal (Fig. 3, F and I). As in previous studies (*48*), $Ca_V1.2$ surface expression is markedly reduced in the absence of β_{2b} subunit (Fig. 3I). By comparison, coexpression of $GeeC_L$ or nb.F3 minimally altered surface-membrane trafficking of $Ca_V1.2$ channels (Fig. 3G-I). Together, these results suggest that $GeeC_L$ enhances $Ca_V1.2$ function by boosting channel openings.

$GeeC_L$ enhances L-type current in cardiomyocytes

Having established the functionality of $GeeC_L$, we sought to determine whether $GeeC_L$ can up-regulate native L-type current in cardiomyocytes. We cultured ventricular cardiomyocytes isolated from adult mice, which primarily express $Ca_V1.2$ channels, and used adenovirus to transduce $GeeC_L$ along with a bicistronically expressed mCherry as fluorescent reporter (Fig. 4A). Whole-cell current recordings show baseline Ca^{2+} currents in these cells evoked in response to a family of voltage-step depolarizations (Fig. 4B). Adenoviral transduction of green fluorescent protein (GFP) revealed a minimal change in J_{peak} (Fig. 4C). By contrast, $GeeC_L$ expression yielded a marked increase in J_{peak} (Fig. 4D) and maximal conductance (fig. S4A). Expression of nb.F3 alone also failed to up-regulate the J_{peak} (Fig. 4E). Analysis of voltage–whole-cell current density relationship revealed a hyperpolarizing ~12-mV hyperpolarizing shift in V_h in the presence of $GeeC_L$ compared to control conditions (fig. S4, B to D). We further analyzed potential changes in channel inactivation by quantifying r_{50}, the amount of current remaining following 50 ms of depolarization at various voltages (fig. S5). We found a modest increase in inactivation in the presence of $GeeC_L$, consistent with previous studies showing enhanced inactivation with full-length Lrrc10 (*36*). One possibility here is that enhanced Ca^{2+} entry through the channels may boost Ca^{2+}-dependent inactivation. These findings demonstrate the ability of $GeeC_L$ to enhance native $Ca_V1.2$ channels in cardiomyocytes.

$GeeC_L$ boosts E-T coupling in neurons in vitro and in vivo

In neurons, $Ca_V1.2/1.3$ channels play an essential role in transducing membrane excitation to changes in gene expression, a process known as E-T coupling. This process is critical for driving neurodevelopmental changes and in modulating synaptic plasticity (*7*, *10*). Briefly, Ca^{2+} entry through *N*-methyl-D-aspartate and $Ca_V1.2/1.3$ channels (*8*, *9*) as well as voltage-dependent conformation changes in the latter (*49*), leads to autophosphorylation of Ca^{2+}/calmodulin-dependent protein kinase II (CaMKII) (*7*). This, in turn, results in activation of downstream pathways and an increase in immediate early genes via phosphorylation of nuclear cyclic AMP response element binding protein (pCREB) (*9*), a transcription factor.

We hypothesized that up-regulation of $Ca_V1.2/1.3$ by $GeeC_L$ may boost E-T coupling. To test this possibility, we transduced either

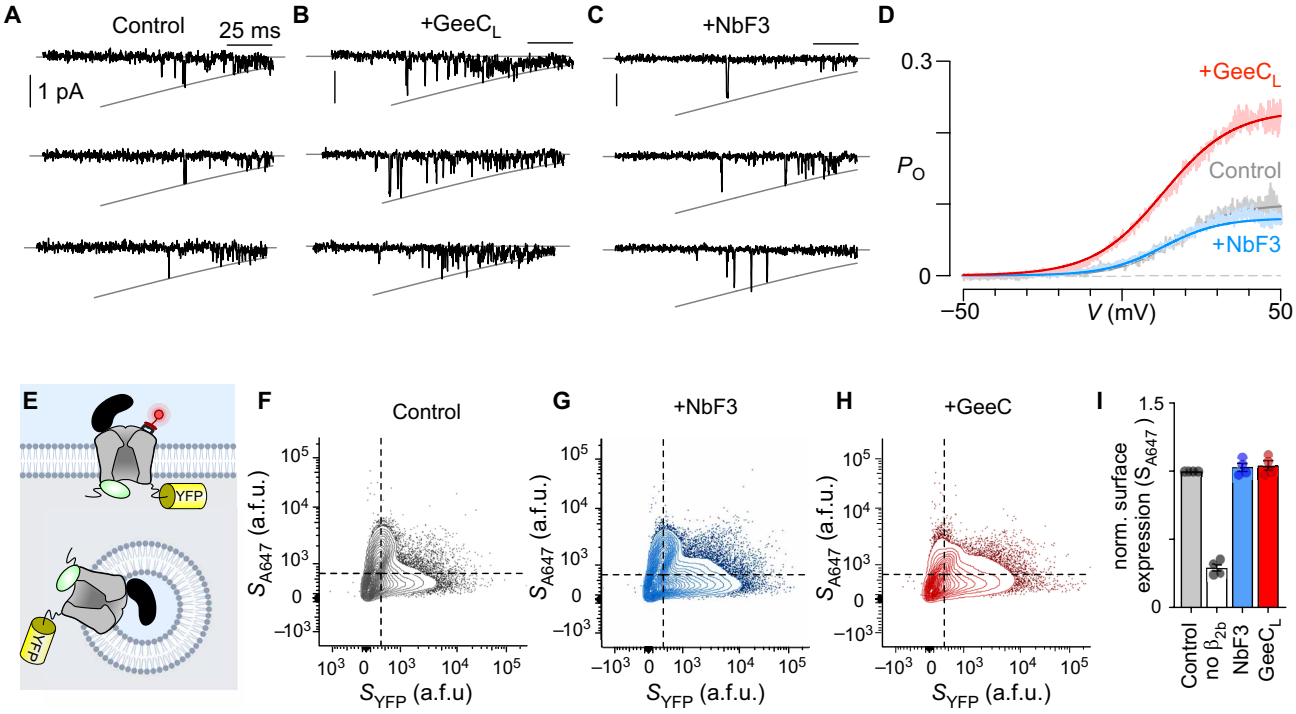

Fig. 3. GeeC$_L$ up-regulates Ca$_V$1.2 function by enhancing channel openings. (**A**) Exemplar cell–attached single-channel recordings of Ca$_V$1.2 reconstituted in HEK 293 cells. Slanted gray curve represents unitary conductance. Each downward deflection indicates channel openings. (**B** and **C**) Coexpression of GeeC$_L$ increases channel openings, while nb.F3 yields minimal change. Format as in (A). (**D**) Ensemble average P_O-voltage relationship for Ca$_V$1.2 shows that GeeC$_L$ increases peak P_O compared to control conditions or in the presence of nb.F3. $n = 6$ (control), $n = 6$ (nb.F3), and $n = 7$ (GeeC$_L$) from three independent transfections. (**E**) Schematic shows dual labeling approach to quantify surface expression of Ca$_V$1.2. The pore-forming α_{1C} subunit is engineered to contain a BTX binding site in DII S5-S6 loop and a YFP at the C terminus. Surface expression can be quantified by labeling with BTX conjugated to Alexa Fluor 647 (S_{A647}), while total expression is determined by measuring YFP fluorescence (S_{YFP}). (**F**) Flow cytometric analysis shows baseline levels of Ca$_V$1.2 surface membrane trafficking in the presence of β_{2b} subunits. (**G** and **H**) Coexpression of GeeC$_L$ (G) or nb.F3 (H) minimally perturbs surface expression of Ca$_V$1.2. (**I**) Population data confirms minimal change in surface-membrane expression of Ca$_V$1.2 in the presence of either GeeC$_L$ (red) or nb.F3 (blue), normalized to control. Each dot represents geometric mean of Alexa Fluor 647 staining from an individual experiment. Bars show mean and SEM. from $n = 4$ transfections.

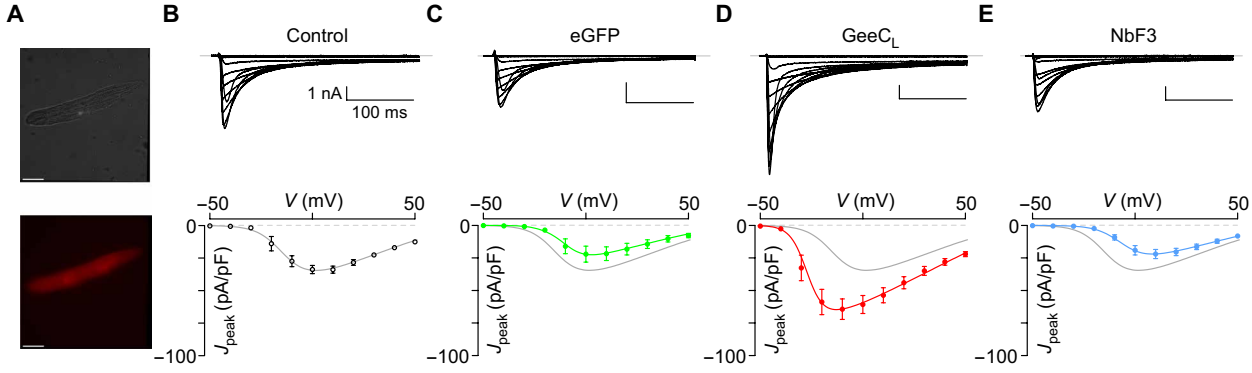

Fig. 4. GeeC$_L$ enhances endogenous Ca$_V$1.2 in mouse-derived cardiomyocytes. (**A**) Brightfield (top) and epifluorescence (bottom) images show a cardiomyocyte expressing GeeC$_L$, with mCherry bicistronically expressed. Scale bars, 10 μm. (**B**) Top: Exemplar traces of endogenous L-type currents in 2-day cultured cardiomyocytes evoked in response to 300-ms voltage steps to various potentials. Bottom: Population data show baseline peak current density. Error bars represent mean and SEM. $n = 11$ cells from three mice. (**C**) Adenoviral expression of GFP minimally perturbs L-type current density. $n = 8$ cells from three mice. Format as in (B). (**D**) GeeC$_L$ markedly up-regulates endogenous L-type channels. $n = 11$ cells from three mice. Format as in (B). (**E**) Nb.F3 by itself failed to appreciably perturb peak current density. Format as in (B). $n = 8$ cells from two mice. eGFP, enhanced GFP.

$GeeC_L$ or GFP into cultured rat hippocampal neurons (Fig. 5). As in previous studies, neurons were depolarized with 40 mM extracellular potassium (K^+) that preferentially evokes signaling through Ca_V1 channels (*8*, *50*). The strength of E-T coupling was then measured by immunostaining of nuclear pCREB. Without depolarization, minimal pCREB was observed in the nucleus (Fig. 5, A and D). Following depolarization, we observed a significant increase in pCREB staining in the nucleus (Fig. 5, A and D). Adenoviral expression of GFP resulted in minimal changes in depolarization-induced pCREB in the nucleus (Fig. 5, B and D). By comparison, expression of $GeeC_L$ resulted in a nearly twofold increase in nuclear pCREB staining compared to uninfected and GFP controls (Fig. 5, C and D). These findings reveal the ability of $GeeC_L$ to augment E-T coupling in cultured neurons, likely reflecting an enhancement in $Ca_V1.2/1.3$ function.

Having confirmed its effect in cultured neurons, we set out to determine whether $GeeC_L$ can boost E-T coupling in the mouse brain. Using stereotaxic surgical techniques, we unilaterally injected 12- to 14-week-old mice with either AAV9-$GeeC_L$ (right hemisphere) or AAV9-GFP (left hemisphere)—as negative control—in the dorsal hippocampus (Fig. 5E) and the medial prefrontal cortex (Fig. 5G). Following 2.5 weeks of recovery, we observed the robust expression of both $GeeC_L$ (mCherry marker) and GFP in the respective hemispheres in the dorsal hippocampus (Fig. 5E) and medial prefrontal cortex (Fig. 5G) brain sections. We probed for pCREB via immunostaining. In the dorsal hippocampus, AAV9-$GeeC_L$–injected hippocampal neurons had higher levels of nuclear pCREB compared to AAV9-GFP control-injected neurons (Fig. 5, F and I). Similar effects were also observed in medial prefrontal cortex (mPFC) neurons, with $GeeC_L$-expressing neurons demonstrating a higher pCREB staining compared to GFP-infected control (Fig. 5, H and I). In all, these findings illustrate the exquisite capability of $GeeC_L$ to modulate E-T coupling in neurons both in vitro and in vivo.

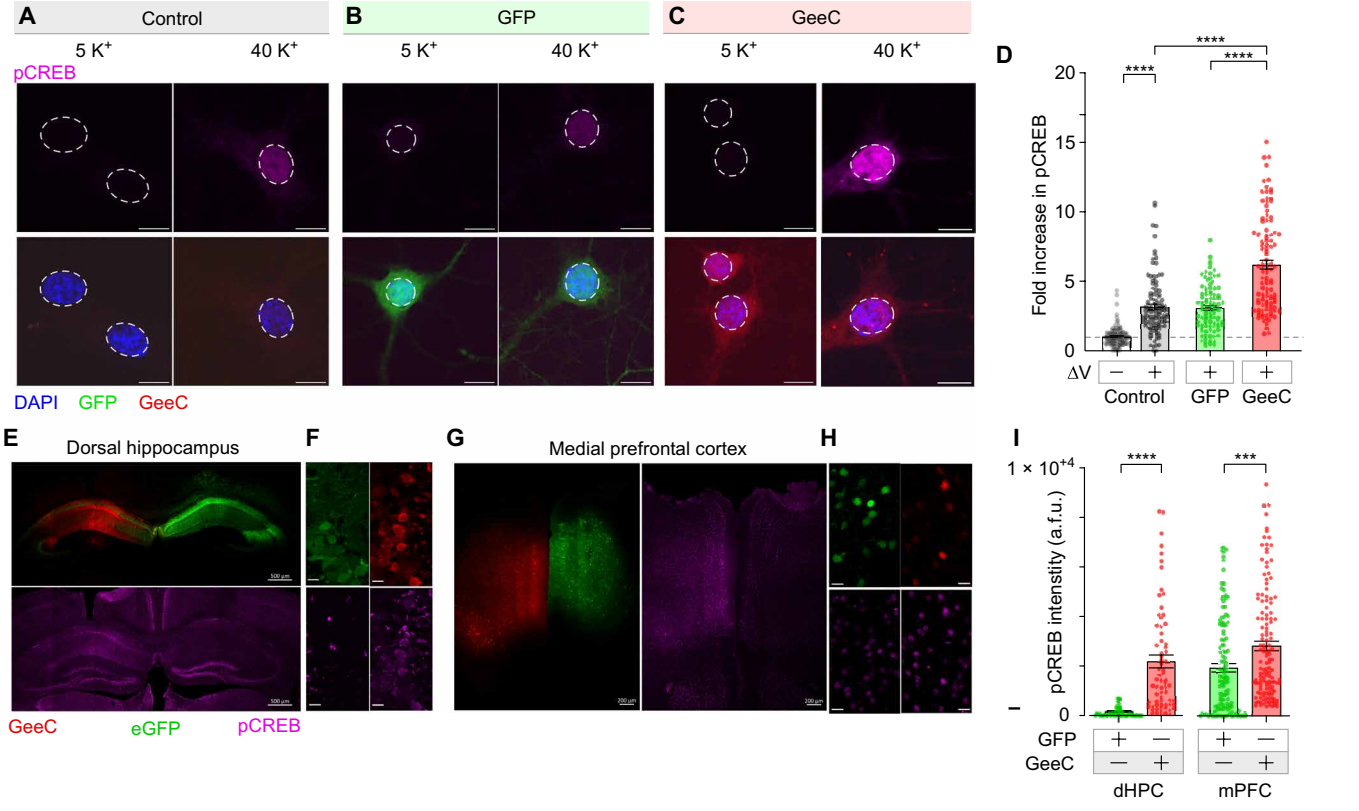

Fig. 5. $GeeC_L$ boosts E-T coupling in neurons. (**A**) Confocal images show increased nuclear accumulation of pCREB (Alexa Fluor 647) following cell depolarization with extracellular solution containing 40 mM K^+. White dashed circles mark the nuclear region for fluorescence quantification based on 4′,6-diamidino-2-phenylindole (DAPI) staining. Scale bars, 5 μm. (**B**) Expression of GFP has minimal effect on nuclear pCREB levels following depolarization. Scale bars, 5 μm. (**C**) Expression of $GeeC_L$ increases nuclear pCREB staining following depolarization. Scale bars, 5 μm. (**D**) Population data compares nuclear pCREB signal following depolarization. Bars show means ± SEM. Statistical analysis: Kruskal-Wallis test followed by Dunn's multiple comparisons test. ****$P < 0.0001$. $n = 133$ (control, resting), $n = 122$ (control; with depolarization), $n = 95$ (GFP), and $n = 110$ ($GeeC_L$) cells from six independent cultures. (**E**) To probe functionality of $GeeC_L$ in vivo, AAV9 encoding either GFP or $GeeC_L$/mCherry was stereotactically injected into the mouse hippocampus. Confocal image of a coronal slice of mouse hippocampi at ×10 magnification shows robust expression of $GeeC_L$ (mCherry) or GFP control AAV9 (top) and pCREB signal (bottom). pCREB staining is qualitatively higher in the right hemisphere with GeeC expression. Scale bars, 500 μm. (**F**) Higher magnification (×40) confocal images of mouse dorsal hippocampal neurons showing GFP (left) or mCherry (right) and corresponding pCREB staining. Scale bars, 20 μm. (**G**) Representative coronal slice of medial prefrontal cortex at ×10 magnification shows either $GeeC_L$ or GFP expression (left) and corresponding pCREB staining (right). Scale bars, 200 μm. (**H**) Higher magnification images of mice prefrontal cortex neurons. Top: GFP or $GeeC_L$ expression. Bottom: pCREB. Scale bars, 20 μm. (**I**) Population data confirms enhanced pCREB staining in $GeeC_L$-expressing prefrontal cortex neurons when compared to GFP-infected controls. Format as in (D). Statistical analysis: Mann-Whitney test. ****$P < 0.0001$.

GeeC$_L$ enhances E-T coupling in Rett syndrome neurons

Rett syndrome (RTT) is an X-linked neurodevelopmental disorder associated with ASD, hypotonia, microcephaly, stereotypical hand movements, and an initial phase of normal development, followed by regression of acquired developmental milestones (*51*). RTT is caused by loss-of-function mutations in methyl CpG-binding protein 2 (MeCP2), a transcriptional regulator. As MeCP2 is a downstream target of L-type Ca^{2+} channels (*52*, *53*) and as decreased gene expression has been reported in RTT (*54*–*57*), we probed whether RTT neurons have altered E-T coupling, and whether modulation of L-type Ca^{2+} channel activity by GeeC$_L$ could perturb this process in the pathophysiological setting. To do so, we leveraged a previously established RTT-like human embryonic stem cell (hESC) line that was genetically engineered from a wild-type female hESC line (*55*, *58*) and differentiated them into neurons in vitro (RTT neurons hereinafter). These RTT neurons have been shown to recapitulate key cellular alterations associated with RTT, including reduced soma size compared to neurons from healthy donors (*55*, *58*) and reduced induction of various intermediate early genes following extracellular K^+-mediated depolarization (*55*). To test if enhancing L-type Ca^{2+} channels with GEEC$_L$ can rescue these features, we infected the neuronal precursor cells derived from this RTT-like hESC with either AAV9-GFP or GeeC$_L$ and then characterized the infected neurons. We first probed baseline changes in E-T coupling in RTT neurons compared to wild-type neurons by measuring nuclear pCREB following depolarization. Compared to control or GFP-expressing wild-type neurons (Fig. 6, A, B, and E), GFP-expressing RTT neurons exhibited markedly reduced nuclear pCREB (Fig. 6, C and E). GeeC$_L$ overexpression reversed this reduction in pCREB to near wild-type levels (Fig. 6, D and E). We additionally tested whether GeeC$_L$ expression could rescue the reduced soma size. Consistent with previous studies (*55*, *58*), Tuj1 staining used to measure soma size revealed ~25% reduction in GFP-expressing RTT neurons compared to wild-type neurons (Fig. 6, F and G and I). Expression of GeeC$_L$ increased soma size, reversing it to near wild-type soma size (Fig. 6, H and I). Together, these findings demonstrate that GeeC$_L$ can boost E-T coupling in RTT neurons and potentially compensate for some signaling deficits in RTT.

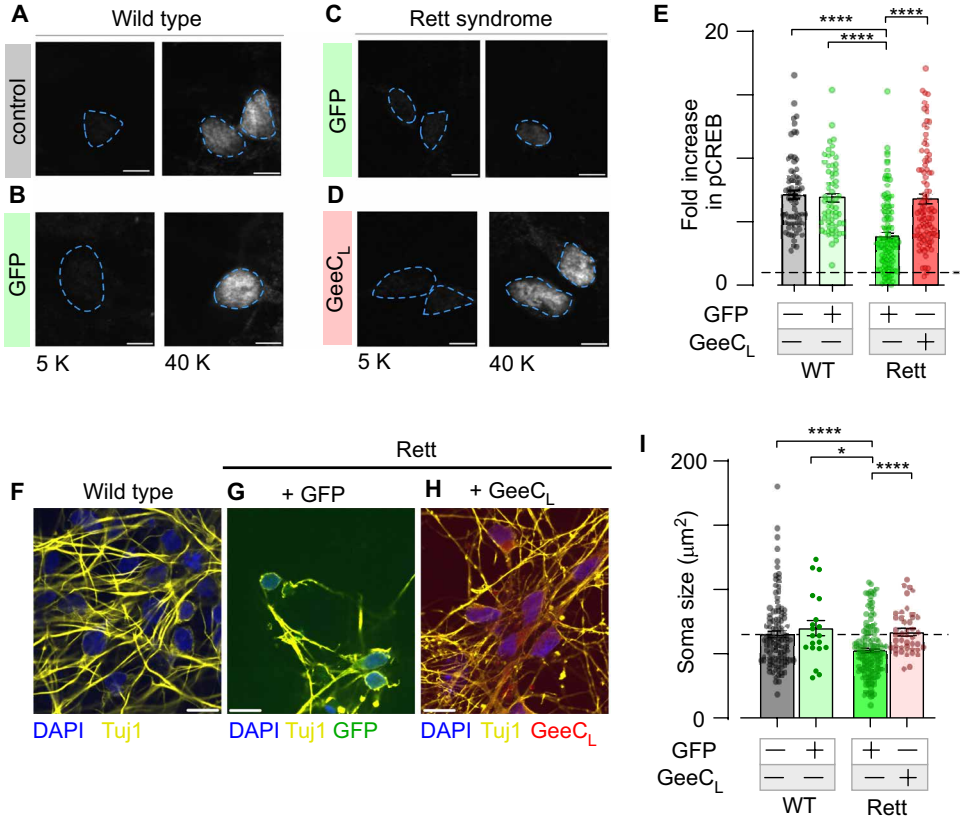

Fig. 6. GeeC$_L$ boosts E-T coupling in RTT neurons. (**A**) Exemplar confocal images show robust increase in nuclear pCREB staining following mild membrane depolarization in wild-type hESC-derived neurons. Left: Baseline. Right: Following 40 mM K^+ stimulation. Scale bars, 5 μm. (**B**) Expression of GFP in wild-type neurons minimally perturbs recruitment of nuclear pCREB. Scale bars, 5 μm. (**C**) Accumulation of pCREB in the nucleus following membrane depolarization is markedly reduced in RTT-like neurons. Scale bars, 5 μm. (**D**) L-type channel up-regulation by GeeC$_L$ enhances pCREB signaling in RTT neurons. Scale bars, 5 μm. (**E**) Bar graph summarizes population data showing increase in pCREB following membrane depolarization in both wild-type and RTT neurons. For statistical analysis, Kruskal-Wallis test followed by Dunn's multiple comparisons test. ****$P < 0.0001$. $n = 73$ (uninfected, wild type), $n = 63$ (GFP, wild type), $n = 128$ (GFP, RTT), and $n = 96$ (GeeC$_L$, RTT) cells from three independent cultures. (**F** to **H**) Confocal images show differences in overall morphology of wild-type (F) versus RTT neurons in the presence of GFP (G) or GeeC$_L$ (H). Blue, DAPI. Yellow: Tuj1. Red, mCherry. Green, GFP. Scale bars, 10 μm. (**I**) Bar graph quantifies changes in soma size in both wild-type and RTT neurons. Each bar and error represents means ± SEM. For statistical analysis, Kruskal-Wallis test followed by Dunn's multiple comparisons test. *$P = 0.0114$ and ****$P < 0.0001$. $n = 44$ (uninfected, wild type), $n = 20$ (GFP, wild type), $n = 155$ (GFP, RTT), and $n = 120$ (GeeC$_L$, RTT) cells from three independent cultures.

DISCUSSION

Precise manipulation of $Ca_V1.2/Ca_V1.3$ in distinct physiological settings is crucial for delineating their biological functions and for broadening their utility as a therapeutic target (*2*). Here, we engineered $GeeC_L$ as a genetically encoded approach to boost $Ca_V1.2/1.3$ function with enhanced specificity in various physiological settings. To do so, we functionalized a nanobody that binds the $Ca_V\beta$ subunit by attaching an effector domain from Lrrc10, an enhancer of Ca_V1 channels. In depth analysis revealed that $GeeC_L$ selectively modulates $Ca_V1.2$ and $Ca_V1.3$ channels by up-regulating P_O while minimally perturbing closely related Ca_V channels. In cardiomyocytes, $GeeC_L$ expression results in increased $Ca_V1.2$ current density, confirming its functionality in modulating native Ca^{2+} channels. Mechanistically, both normalized tail current measurements and single-channel recordings in HEK 293 cells suggest that $GeeC_L$ minimally perturbs the voltage dependence of $Ca_V1.2$ activation. In cardiomyocytes, however, we found that $GeeC_L$ evoked a hyperpolarizing shift in V_h. One possibility is that endogenous $Ca_V1.2$ in cardiomyocytes are heterogenous macromolecular complexes composed of distinct regulatory proteins and variable baseline P_O and V_h. In this scenario, it is possible that $GeeC_L$ may disproportionally affect select channel subpopulations, which could lead to an apparent shift in voltage dependence of channel activation. In cultured hippocampal neurons, we found that $GeeC_L$ expression increased pCREB staining, suggesting enhanced E-T coupling. Furthermore, $GeeC_L$ delivery into mouse hippocampus and medial prefrontal cortex increased pCREB in neurons, pointing to enhanced E-T coupling in vivo. Thus, $GeeC_L$ provides an avenue to up-regulate $Ca_V1.2/1.3$ function in various physiological settings.

Several pharmacological Ca_V1 blockers, including dihydropyridines and verapamil, are routinely used clinically to down-regulate Ca_V1 activity for various indications (*2*). Although $Ca_V1.2/1.3$ agonists have been postulated as potential treatment for multiple diseases including bladder dysfunction (*59*), these approaches pose inherent challenges. Previous studies that used Bay K 8644, a dihydropyridine, in rodents reported increased coronary vascular resistance, self-biting behavior, and motor abnormalities including twisting and stretching movements, limb extension, back arching, spasticity, and ataxia (*29*–*31*). A key advantage of $GeeC_L$ is that it is genetically encoded and may be delivered to specific cell types using emerging viral gene delivery approaches (*60*). From a biological perspective, $GeeC_L$ may provide a convenient strategy to dissect the functional contribution of $Ca_V1.2/1.3$ channels in various physiological or pathophysiological settings. In the present study, application of $GeeC_L$ revealed that boosting L-type channel function can compensate for some pathophysiological signaling changes in a neuronal model of Rett syndrome. Specifically, RTT neurons show a baseline reduction in E-T coupling, which could be reversed by expression of $GeeC_L$. These findings are consistent with previously reported reduction in activity induced expression of intermediate early genes in these cells (*55*) and reduced CREB signaling in similar cell lines and mice (*61*). Up-regulation of $Ca_V1.2/1.3$ function by $GeeC_L$ also reversed deficits in soma size, a cellular phenotype of RTT neurons. Previous work has shown that up-regulating CREB signaling, downstream of Ca_V1 activation, in RTT neurons can enhance neurite outgrowth and dendritic complexity (*61*). It is currently unknown whether there are deficits in $Ca_V1.2/1.3$ function in RTT neurons. Gene expression analysis has shown reduced expression of both $Ca_V\beta_1$ and $Ca_V\beta_3$ subunits in MeCP2 null mice (*56*) and in hESC-derived RTT neurons (*57*). Conversely, expression of both $Ca_V\beta$ subunits is increased in MeCP2-overexpressing models (*56*). Nevertheless, it is possible that up-regulation of $Ca_V1.2/1.3$ by $GeeC_L$ may be compensatory for other signaling changes. RTT is a complex disorder involving a myriad of transcriptional changes and cell type–specific effects including imbalance of neuronal excitation and inhibition as well as altered astrocyte Ca^{2+} signaling (*62*–*64*). Therefore, it is unlikely that $GeeC_L$ would be able to reverse all these changes from a therapeutic perspective. Instead, $GeeC_L$ may provide a targeted approach for studying how alterations in L-type channel function can affect this complex system. More broadly, in the brain, inducible expression of $GeeC_L$ in distinct neuron populations or specific neural circuits may allow us to delineate the complex contribution of Ca_V1 function to elicit a variety of behavioral responses in animal models or to dissect the importance of Ca_V1 in formation of neural circuits in the developing brain through inducible expression in early developmental stages (*65*). In the heart, $GeeC_L$ could be used to selectively target $Ca_V1.2$ in cardiomyocytes, potentially increasing E-C coupling, inotropy, and cardiac output. This may be advantageous to delineate the discrete roles for augmented Ca^{2+} entry versus phosphorylation in heart remodeling and cardiac disease, where prolonged adrenergic stimulation plays a pathophysiological role (*66*, *67*).

Our findings also provide insights on the mechanism of Lrrc10 modulation of Ca_V1 channels and beyond. Lrrc10 is an evolutionarily conserved protein that is exclusively expressed in cardiomyocytes (*68*). In zebrafish, Lrrc10 is essential for cardiac function, including cardiac development (*40*). Specifically, Lrrc10 knockdown leads to reduced cardiomyocyte population and cardiac dysmorphism. In mice, deletion of Lrrc10 results in reduced cardiac function immediately after birth, progressing to dilated cardiomyopathy in adulthood (*68*, *69*). In addition, these mice exhibit poor cardiac tolerance to pressure overload induced by transverse aortic constriction (*42*). Furthermore, human Lrrc10 variants are associated with pediatric dilated cardiomyopathy (*36*, *70*) and cardiac arrhythmias (*71*). Recently, Lrrc10 has also been found to be an essential element for heart regeneration in both zebrafish (*39*, *40*) and in mammals (*41*); however, how Lrrc10 mediates this effect is not fully understood. Lrrc10 is known to associate with multiple proteins, including the α subunit of the $Ca_V1.2$ channel (*36*), α-actinin (*69*), and actin (*69*). Here, we find that the high affinity interaction with $Ca_V1.2$ is mediated by the Lrr domains, similar to Lrrc10 interaction with other targets. Lrr domains are thought to mediate protein-protein interactions and may promiscuously support association with diverse targets (*43*). Critically, functional $Ca_V1.2$ up-regulation also requires the NT of Lrrc10, which may serve as a low-affinity effector domain. Disease-linked human variants in Lrrc10 such as I195T are, however, localized within the Lrr domains. One possibility is that these variants may alter the conformation of Lrrc10 binding which may allosterically alter the interaction of Lrrc10 NT. Unlike the Lrr domains that share considerable homology with other Lrrc family of proteins (*68*), the NT region is unique to Lrrc10 and is highly conserved across species. This suggests that while other members of the Lrrc family of proteins may also interact with the $Ca_V1.2$ channel, it is unlikely that these proteins would serve as $Ca_V1.2/1.3$ agonists. Further studies are necessary to identify the channel interfaces responsible for

binding of both Lrr and the NT effector domains. One intriguing possibility is the potential binding of Lrrc10 to the C-terminal domain of Ca_V1 channels, which serves as a nexus for interacting with other regulatory proteins, including calmodulin and stac proteins, both of which up-regulate Ca_V1 P_O (*72*, *73*). Our findings also suggest that Lrrc10 can interact with $Na_V1.5$ and result in increased I_{NaL} when overexpressed in HEK cells. It is currently unknown whether Lrrc10 associates with endogenous $Na_V1.5$ in cardiac myocytes, and if so, whether this could lead to increased I_{NaL} in the native setting. Furthermore, it is not currently known how human disease-linked variants in Lrrc10 affect $Na_V1.5$ regulation. It is possible that the full consequence of Lrrc10 dysfunction may involve altered regulation of multiple ion channels and other proteins.

From a molecular engineering perspective, $GeeC_L$ is a versatile and generalizable platform to devise $Ca_V1.2/1.3$ actuators with desired properties. Although Lrrc10 itself can up-regulate $Ca_V1.2$ currents, its modulation of other proteins including $Na_V1.5$ limits its potential as a targeted enhancer of $Ca_V1.2$. Our current design targets the $Ca_V\beta$ subunit to modulate channel function. As there are differences in cytosolic domains of $Ca_V1.2$ versus $Ca_V1.3$, it may be possible to engineer nanobodies that target the channels directly. At present, $GeeC_L$ is a constitutive enhancer of Ca_V1. However, it may be feasible to engineer $GeeC_L$ such that Lrrc10 NT is recruited to the targeting domain (i.e., nanobody) through chemically induced (*74*) or optogenetic dimerizers (*75*). More broadly, nanobodies have emerged as a powerful platform to probe and manipulate ion channel function. Nanobodies have been functionalized through attachment of fluorescent reporters (*76*) or enzymes that alter channel posttranslational modifications to tune channel localization (*28*, *45*). Our findings suggest that low-affinity functional domains from channel interacting proteins or other targets could also be used as payloads for tuning specific aspects of channel function. This strategy may be advantageous, as recent studies have identified a number of short peptides that tune specific properties of Ca_V and Na_V channels (*73*, *77*).

Limitations

Two caveats merit further attention. First, the effectiveness of $GeeC_L$ relies on two factors, (i) the high affinity of NbF3 for $Ca_V\beta$ and (ii) the weak affinity of the Lrrc10 NT for $Ca_V1.2$ itself. This strategy allows $GeeC_L$ to circumvent the off-target effects of Lrrc10 overexpression with $Na_V1.5$. Nevertheless, it is possible that under high overexpression conditions, $GeeC_L$ could still associate with other targets, leading to nonspecific effects. Second, the structure of Lrrc10 is currently unsolved. In AlphaFold3 predictions, segments of the Lrrc10 NT appear to be a part of the integral fold of Lrrc10 (*78*). Thus, it is possible that truncating Lrrc10 into NT and CT fragments may have perturbed folding, leading to reduced affinity for $Ca_V1.2$, while in the holo-Lrrc10 structure, this domain may still exhibit a high affinity for $Ca_V1.2$.

Conclusions

In all, $GeeC_L$ enables targeted up-regulation of $Ca_V1.2/1.3$ channels in diverse physiological settings, thereby opening avenues to development of future therapeutics and providing a convenient strategy to systematically dissect the function of these channels in a cell type–dependent manner.

MATERIALS AND METHODS

Ethical statement

All animal experimental procedures were carried out in accordance with regulations and established guidelines and were reviewed and approved by the Institutional Animal Care and Use Committees at Columbia University (AC-AABI1550) and at Weill Cornell (2010-0004).

Molecular biology

We synthesized $GeeC_L$ as a DNA fragment by isolating the first 53 amino acids of human LRRC10 and linking them to nb.F3-P2A peptide through a GSGRSGSG sequence, flanked by Nhe I/Eco RI sites (Twist Bioscience). The gene fragment was ligated using T4 DNA ligase (Thermo Fisher Scientific) into a PiggyBac cytomegalovirus (CMV) mammalian expression vector that encoded a cyan fluorescent protein (CFP) sequence downstream of a P2A peptide. Ligates were then transformed into either XL10-Gold Ultracompetent Cells (Agilent) or DH5a Competent Cells (Thermo Fisher Scientific), plated, and cultured in selective LB broth or CIRCLEGROW Medium (MP Biomedicals). DNA was extracted and purified from cultures using either the QIAprep Spin Miniprep Kit (QIAGEN) or GeneJET PCR Purification Kit (Thermo Fisher Scientific). Sanger (Eton Bioscience Inc. and Genewiz from Azenta Life Sciences) and Nanopore sequencing (SNPsaurus LLC) were used to verify plasmids. FRET plasmids were generated by polymerase chain reaction amplification of full-length human LRRC10, LRRC10 NT, and LRRC10 LRR1 CT using primers flanked by restriction sites Nhe I or Bgl II/Sal I. Sequences were then ligated into a pcDNA3 plasmid coding for a downstream GSG-Cerulean (Cer) sequence immediately after restriction site.

Adenovirus and AAV generation

Plasmids, adenovirus (pAV[Exp]-mCherry-CMV>[$GEEC_L$] and pAV[Exp]-CMV>EGFP) and AAV9 (pAAV[Exp]-CMV>[$GEEC_L$]:BGHpA-hPGK>mCherry:WPRE and pAAV[Exp]-CMV>EGFP:-WPRE) were constructed and packaged by VectorBuilder. CFP-P2A-nb.F3 adenovirus was used as in previous studies.

HEK 293 cell culture and transfection

HEK 293 cells (American Type Culture Collection, catalog no. CRL1573) were cultured on glass coverslips in 60-mm dishes and transfected using a calcium phosphate method. For whole-cell electrophysiology, we applied 4 μg of cDNA encoding rabbit α_{1C} subunit (NM_001136522) along with 4 μg of human β_{2b} subunit (AF285239.2) and 4 μg of rat brain $\alpha_2\delta_1$ (NM_012919.2). We cotransfected 4 μg of either $GeeC_L$ or nb.F3 in experiments that required so. To enhance expression, cDNA for simian virus 40 T antigen (0.5 mg) was cotransfected. Electrophysiology recordings were done at room temperature 24 hours after transfection. For single-channel electrophysiology, we applied 1 μg of α_{1C}, β_{2b} and $\alpha_2\delta_1$, along 1 μg of either $GeeC_L$ or nb.F3. For total and surface Ca^{2+} channel flow cytometric assay, we transfected 3 μg of engineered α_{1C} and β_{2b} subunits along with either nb.F3 or $GeeC_L$. To enhance expression, cDNA for simian virus 40 T antigen (0.5 mg) was cotransfected.

Cardiomyocyte isolation, culture, and infection

Mice ventricular myocytes were isolated from 8- to 12-week-old nontransgenic (C57BL/6) mice by enzymatic digestion using a

Langendorff perfusion apparatus. Both male and female mice were used to obtain isolated cardiomyocytes, and experimental outcomes were unaffected by sex. Cardiomyocytes were resuspended in perfusion solution with 5% fetal bovine serum (General Electric). $CaCl_2$ was added over 30 min to a final concentration of 1 mM. Cells were plated on glass coverslips precoated with laminin (Corning). Plating medium contained minimal essential medium (MEM) with Earle's salts and L-glutamine, 5% fetal bovine serum, 1% penicillin-streptomycin and 10 mM 2,3-butanedione monoxime (BDM). Cardiomyocytes were allowed to precipitate and adhere for 2 hours before changing to maintenance medium, which contained MEM with Earle's salts, L-glutamine, 1% penicillin-streptomycin, bovine serum albumin (0.5 mg ml^{-1}), 10 mM BDM, 1% insulin-transferrin-selenium, 5 mM creatine, 5 mM taurine, 2 mM L-carnitine, and 25 μM blebbistatin. For deployment of $GeeC_L$, nb.F3, or GFP, 1 to 2 μl of adenovirus were resuspended in the culture medium at least 2 hours after cell plating. Maintenance medium was replaced after 12 to 20 hours to reduce potential adenoviral toxicity. Viral transduction efficacy was assessed 24 to 48 hours after infection. Only non-contracting, rod-shaped cardiomyocytes with clear striations were used for electrophysiology.

Isolated rat hippocampal neuron culture and infection

Culturing kits for rat hippocampi at embryonic age 18 were procured from Transenetyx Tissue by BrainBits (Transnetyx Inc.). Neurons were isolated from hippocampi using papain in Ca^{2+}-free medium (2 mg/ml) and gentle mechanical dissociation. Cells were plated in 12-well plates containing glass cover slips precoated with poly-D-lysine (50 μg/ml) at a final concentration of 16,000 cells/cm^2. Neurons were cultured initially in NbActiv1 culture medium (BrainBits) and switched to Neurobasal/B27/GlutaMAX "maintenance" medium (Gibco) 96 hours after plating. Medium changes were done subsequently every 72 hours. $GeeC_L$ and GFP were adenovirally transduced on culture day 10 by resuspending 0.5 to 1 μl of adenovirus in culture medium; medium was replaced 12 to 20 hours after infection. Transduction efficiency was evaluated 72 to 96 hours after infection.

RTT-like hESC and neuronal differentiation

Human ESCs were cultured on irradiated mouse embryonic fibroblasts with standard hESCs medium: [Dulbecco's modified Eagle's medium (DMEM)/F12 (Invitrogen) supplemented with 15% fetal bovine serum (FBS) (Gibco HI FBS, 10082-147), 5% KnockOut Serum Replacement (Invitrogen), 2 mM L-glutamine (MPBio), 1% nonessential amino acids (Invitrogen), 1% penicillin-streptomycin (Lonza), 0.1 mM β-mercaptoethanol (Sigma-Aldrich), and fibroblast growth factor (FGF2) (4 ng/ml; R&D Systems)]. To differentiate hESC into neurons, two or three wells of confluent cells from six-well plate are treated with Rho-associated protein kinase inhibitor overnight. The cells were washed with phosphate-buffered saline (PBS) once and then treated with collagenase IV (1 mg/ml) for 45 min. The harvested hESC aggregates were collected and grew on a nonadherent six-well plate for 5 days with Noggin (500 ng/ml) and SB-431542 (10 μM) in DMEM/F12 medium, and then the SB-431542 was removed for another 2 days. For the next 7 days, the cells were treated with FGF (20 ng/ml). To harvest, cells were washed with PBS and incubated for 10 min with PBS with EDTA, then incubated for 10 min with Accutase, harvested to prepare droplet plate onto poly-ornithine–/laminin-coated plates, and incubated in 37°C incubator for 2 hours followed by adding 5 ml of medium for each well. To differentiate these neuronal precursor cells into neurons, we withdrew FGF and grew them on Matrigel-coated plate in DMEM/F12 for 2 to 4 weeks to promote maturation.

Whole-cell electrophysiology

Whole-cell voltage-clamp recordings for HEK 293 were collected at room temperature using an Axopatch 200B amplifier (Axon Instruments). Glass pipettes were pulled with a horizontal puller (P97; Sutter Instruments Co.) and fire-polished (Microforge, Narishige, Tokyo, Japan), resulting in 2- to 5-megohm resistances, before series resistance compensation of 70%. Internal solutions in experiments performed in HEK 293 cells contained 135 mM $CsMeSO_3$, 5 mM $CsCl_2$, 1 mM $MgCl_2$, 4 mM MgATP, 10 mM Hepes, and 10 mM 1,2-bis(2-aminophenoxy)ethane-*N*,*N*,*N*′,*N*′-tetraacetic acid (BAPTA). Internal solutions in experiments performed in cultured cardiomyocytes contained 114 mM $CsMeSO_3$, 5 mM $CsCl_2$, 1 mM $MgCl_2$, 4 mM MgATP, 10 mM Hepes, 10 mM BAPTA, and 5 μM ryanodine. Internal solutions were adjusted to 290 to 295 mOsm with $CsMeSO_3$ and to pH 7.4 with CsOH. For experiments measuring Ca_V1 currents expressed heterologously in HEK 293 cells, the external solution contained 140 mM TEA-$MeSO_3$, 10 mM Hepes (pH 7.4), and 40 mM $BaCl_2$. For experiments measuring Ca_V2 currents expressed heterologously in HEK 293 cells, the external solution contained 140 mM TEA-$MeSO_3$, 10 mM Hepes (pH 7.4), and 5 mM $BaCl_2$. For experiments measuring L-type currents in cultured cardiomyocytes, the external solutions contained 140 mM TEA-$MeSO_3$, 10 mM Hepes (pH 7.4), and 5 mM $CaCl_2$. External solutions were adjusted to 300 mOsm with TEA-$MeSO_3$ and pH 7.4 with TEA-OH. Individual cells with no adjacent contacts were selected for recordings. In HEK 293 cells, peak currents were determined by measuring steady-state currents after 15-ms test pulses from −50 to +90 mV. For experiments involving cardiomyocytes, cultured cells were incubated 10 min before recordings in a bath solution containing 140 mM TEA-$MeSO_3$, 10 mM Hepes (pH 7.4), 5 mM $CaCl_2$, and 5 μM ryanodine. Currents were elicited by 300-ms depolarization at −50 to +50 mV. Custom MATLAB (MathWorks) software was used to determine peak currents. Normalized tail current recordings were fit using: $I_{norm} = 1/\{1 + \exp.[-(V - V_h)/SF]\}$, where V_h and SF are fit parameters. J_{peak}–voltage (V) relationship was fit using: $J_{peak} = G_{max} * 1/\{1 + \exp.[-(V - V_h)/SF]\} * (V - V_{rev})$, where G_{max}, V_h, V_{rev} are fit parameters corresponding to maximal conductance, half-activation voltage, and reversal potential, respectively. In both cases, fit parameters and 95% confidence interval were determined using the nlinfit function (MATLAB).

Flow cytometric FRET 2 hybrid assay

HEK 293 T cells were cultured in 12-well plates and transfected with polyethylenimine (Polysciences Inc.) or FuGENE 4 K (Promega). LRRC10-Cer and holo-CaV1.2 venus (Ven)–tagged cDNA pairs (20 ng and 2 μg, respectively) were mixed in serum-free DMEM media. FRET experiments were performed 3 to 5 days after transfection. Cycloheximide was added to wells at a final concentration of 100 μM 2 hours before flow cytometric evaluation to halt new fluorophore synthesis and allow for maturation of existing fluorophores. FRET measurements were done using LSR II (BD Biosciences) flow cytometer, equipped with 405-nm, 488-nm, and 633-nm lasers for excitation and 18 different emission channels. Analysis was performed as described (*34*).

Single-channel electrophysiology

Pipettes were pulled from ultrathick-walled borosilicate glass (BF200-116-10, Sutter Instruments) as described in previous section, resulting in resistances of 5 to 10 megohm. To reduce noise, pipettes were distally coated with Sylgard (Dow Corning). External solution contained 132 mM K^+-glutamate, 5 mM KCl, 5 mM NaCl, 3 mM $MgCl_2$, 2 mM EGTA, 10 mM glucose, 20 mM Hepes at 300 mOsm adjusted with glucose and pH 7.4 adjusted with NaOH. Internal solution contained 140 mM TEA-$MeSO_3$, 10 mM Hepes (pH 7.4), and 40 mM $BaCl_2$, adjusted to 300 mOsm with TEA-$MeSO_3$ and pH 7.4 with TEA-OH. Solutions were chosen on the basis of previous studies (*72*). Single-channel opening was elicited during a 200-ms voltage ramp from −80 to +60 mV. For each patch, 100 to 200 sweeps were recorded. Number of channels per recording were then determined by obtaining additional 80 to 150 sweeps after addition of Bay K 8644 to the external solution (final concentration of 9 μM). Ensemble average traces were fit using a Boltzmann Relation: $P_O = P_{O,max} * 1/\{1 + \exp.\ [-(V - V_h)/SF]\}$, where $P_{O,max}$, V_h, and SF are fit parameters.

Total and surface calcium channel flow cytometric assay

We evaluated total and surface Ca^{2+} channel populations using flow cytometry in live, HEK 293 cells as in previous studies (*48*). Briefly, transfected HEK 293 cells cultured in 12-well plates were gently washed with ice-cold PBS containing Ca^{2+} and Mg^{2+} [0.9 mM $CaCl_2$ and 0.49 mM $MgCl_2$ (pH 7.4)] 72 to 96 hours after transfection. Cells were then blocked for 30 with DMEM containing 3% bovine serum albumin at 4°C, followed by 1 hour incubation in DMEM/3% bovine serum albumin containing 1 μM Alexa Fluor 647 conjugated α-BTX (Life Technologies) at 4°C. HEK 293 cells were then rinsed thrice with PBS containing Ca^{2+} and Mg^{2+}. Cells were harvested in Ca^{2+}-free PBS and evaluated by flow cytometry using a BD Fortessa Cell Analyzer (BD Biosciences). Data were analyzed using FlowJo flow cytometry analysis software (BD Biosciences).

Isolated neuron stimulation

All experiments were performed on culture days 14 to 16. Following a previously validated protocol, neurons were pretreated with 1 μM TTX, 10 μM D,L-2-amino-5-phosphonovaleric acid (APV), and 10 μM 2,3-dihydroxy-6-nitro-7-sulfamoylbenzo[*f*]quinoxaline 6-nitro-7-sulfamoylbenzo[*f*]quinoxaline-2,3-dione (BQX) resuspended into culture medium to prevent spontaneous depolarization and block glutamate-driven neurotransmission. After 4 hours, glass coverslips were transferred to a resting solution containing 150 mM NaCl, 4 mM KCl, 2 mM $MgCl_2$, 2 mM $CaCl_2$, 10 mM Hepes, and 10 mM glucose at pH 7.4 (balanced with NaOH). Neurons were stimulated for 3 min by transferring coverslips into a solution containing 114 mM NaCl, 40 mM KCl, 2 mM $MgCl_2$, 2 mM $CaCl_2$, 10 mM Hepes, and 10 mM glucose at pH 7.4 (balanced with KOH). Resting and stimulation solutions also contained 1 μM TTX, 10 μM APV, and 10 μM NBQX (*49*). Neurons were then transferred to fixing solution as described in immunocytochemistry section.

Immunocytochemistry

We fixed isolated neurons using ice-cold 4% paraformaldehyde in PBS with Ca^{2+} and Mg^{2+}, 4% sucrose, and 20 mM EGTA. Cells were then permeabilized with 0.1% Triton X-100 (Sigma-Aldrich) and blocked for 1 hour with 10% HyClone fetal bovine serum (General Electric) in PBS with Ca^{2+} and Mg^{2+}. Neurons were then incubated overnight at 4°C in 1% bovine serum albumin in PBS with pCREB (Ser^{133}) (87G3) Rabbit monoclonal antibody (mAb) (1:333; Cell Signaling Technology, catalog no. #9198). Neurons were then thrice rinsed with PBS, followed by 1-hour incubation with secondary antibody [anti-Rabbit Alexa Fluor 647 (1 mg/ml); Thermo Fisher Scientific] and thrice rinsing with PBS again. Coverslips were then mounted using 4′,6-diamidino-2-phenylindole (DAPI)–containing mounting solution and stored at 4°C (*49*, *79*).

Stereotaxic surgery

Twelve- to 14-week-old C57BL/6 male mice (the Jackson Laboratories, Bar Harbor, Maine) were placed on a stereotaxic surgical apparatus unit (David Kopf Instruments, Tujunga, CA). A midline incision was made on the scalp, and the head was leveled on the basis of bregma and lambda. Mice were injected unilaterally in the dorsal hippocampus ($n = 2$) and the mPFC ($n = 3$) with two different viruses using a 2.5 μl of 30-gauge Hamilton syringe. The right hemisphere received 400-nl injection of AAV9-pAAV[Exp]-CMV[$GEEC_L$]-mCherry and the left hemisphere received 400-nl injections of AAV9-pAAV[Exp]-CMV-EGFP control virus for both brain regions at 0.1 μl/min. Coordinates for the PFC [anteroposterior (AP) = 2.0, dorsoventral (DV) = −2.3, mediolateral (ML) = ±0.3) and dorsal hippocampus (AP = −1.85, DV = −1.55, ML = ±1.10) were based on the Allen Brain Atlas. The needle was left in place for an additional 5 min after the infusion to ensure that the virus was completely delivered before switching to the needle with the second virus. After 2.5 weeks of recovery, mice were given a ketamine/xylazine cocktail at 10 mg/kg and perfused with 1X PBS (pH 7.4) with heparin, followed by an infusion of 4% paraformaldehyde (pH 7.4). Brains were postfixed overnight in 4% paraformaldehyde at 4°C and were sectioned the next day using a Leica vibratome at 40-μm thickness.

Immunohistochemistry

Brain sections were evaluated for expression of mCherry for confirmation of AAV9-$GeeC_L$ and GFP for AAV9-GFP viral infection. After confirmation of expression, tissue sections were washed 3× for 10 min in 1X PBS. Tissue was then blocked in a solution of 1X PBS/3% normal goat serum/0.1% Triton X-100 for 1 hour at room temperature, followed by 3× washes for 10 min in 1X PBS. pCREB (Ser^{133}) (87G3) Rabbit mAb (Cell Signaling Tehcnology, catalog no. #9198) was diluted in 1X PBS/1% bovine serum albumin/0.1% Triton X-100 (1:1000) followed by overnight incubation at 4°C. The following day, tissue was rinsed 3× in 1X PBS for 10 min and then incubated in Donkey anti-Rabbit IgG (H+L) Highly Cross-Adsorbed Secondary Antibody, Alexa Fluor 647 (1:500; Thermo Fisher Scientific, catalog no. A-31573). Tissue was rinsed 3× in 1X PBS for 10 min and then mounted on glass slides and coverslipped with ProLong Glass Antifade Mountant with NucBlue Stain (Invitrogen, catalog no. P36981). Slides were left to rest in the dark overnight before imaging.

Image acquisition and analysis

We imaged fixed cultured rat neurons using a 60× (1.3 NA) oil objective on a Nikon Ti Eclipse inverted microscope equipped with a Yokogawa CSU-X1 confocal spinning disk and an Andor Zyla scientific complementary metal-oxide semiconductor camera. ImageJ

[National Institutes of Health (NIH)] was used to quantify signal intensity, and we selected for analysis only neurons expressing either mCherry (for $GeeC_L$) or GFP; uninfected controls were selected using DAPI signal. In each field of view, we selected a cell-free region of interest as signal background, and we subtracted its mean intensity from all regions of interest. Analysis of nuclear pCREB was done by manually drawing the nuclear regions while viewing only DAPI, GFP, and red fluorescent protein channels but blinded to the pCREB color channel (647 nm). We then quantified background-subtracted mean intensity and normalized it to unstimulated condition (*49*). Brain slice images were acquired for the mCherry, GFP, and Cy5 (detection of pCREB) channels using a Zeiss LSM 880 Laser Scanning Confocal Microscope. All channels, laser intensities, gains, and detection ranges were kept consistent between scans. GFP [488 laser (excitation, 488; emission, 525) with detection range of 500 to 550] was used to visualize the cells infected with the AAV9-GFP reporter control, DSRed [561 laser (excitation, 561; emission, 603) with detection range of 580 to 625)] was used to image cells infected with AAV9-$GeeC_L$-mCherry, and the Cy5 channel [633 laser (excitation, 633; emission, 695) with detection range of 640 to 750)] was used to see expression of pCREB after immunohistochemistry. Images were taken as a z stack, with bidirectional X and four frames averaging. The 488/561/633 filter was used. After acquisition at ×40 and ×20 magnification, images were processed for quantification using Fiji/ImageJ. One z-stack from each scan was chosen and placed through automatic thresholding of the $GeeC_L$/GFP channels. Using analyze particles, automatic regions of interest (ROIs) were made around the soma of each $GeeC_L$/GFP-tagged neuron and added to the ROI manager. Alongside, automatic ROIs were created for the background to use as a normalizer for the corrected total cell fluorescence (CTCF). Area, integrated density and mean gray values were calculated for all preset ROIs in the respective pCREB/Cy5 channel stack. CTCF was calculated using integrated density – (area * mean background gray value) to normalize pCREB intensity values for the respective background around each ROI. An unpaired *t* test was performed using GraphPad Prism to compare CTCF of pCREB in $GeeC_L$ and GFP-tagged neurons. Results were considered significant with a P value < 0.05.

Statistical analysis

All statistical analysis was performed using GraphPad Prism 10. For multiple comparisons, we used one-way analysis of variance (ANOVA) followed by multiple comparisons testing. For comparisons of two groups, we used unpaired two-tail *t* tests.

Supplementary Materials

This PDF file includes:

Supplementary Text
Figs. S1 to S5

REFERENCES AND NOTES

1. B. Hille, *Ionic channels of excitable membranes* (Sinauer Associates, ed. 3, 2001), pp. 814.
2. G. W. Zamponi, J. Striessnig, A. Koschak, A. C. Dolphin, The physiology, pathology, and pharmacology of voltage-gated calcium channels and their future therapeutic potential. *Pharmacol. Rev.* **67**, 821–870 (2015).
3. F. Hofmann, V. Flockerzi, S. Kahl, J. W. Wegener, L-type CaV1.2 calcium channels: From in vitro findings to in vivo function. *Physiol. Rev.* **94**, 303–326 (2014).
4. D. M. Bers, Cardiac excitation-contraction coupling. *Nature* **415**, 198–205 (2002).
5. O. Vivas, C. M. Moreno, L. F. Santana, B. Hille, Proximal clustering between BK and Ca(V)1.3 channels promotes functional coupling and BK channel activation at low voltage. *eLife* **6**, e28029 (2017).
6. N. V. Marrion, S. J. Tavalin, Selective activation of Ca^{2+}-activated K^+ channels by co-localized Ca^{2+} channels in hippocampal neurons. *Nature* **395**, 900–905 (1998).
7. R. Dolmetsch, Excitation-transcription coupling: Signaling by ion channels to the nucleus. *Sci. STKE* **2003**, PE4 (2003).
8. D. G. Wheeler, R. D. Groth, H. Ma, C. F. Barrett, S. F. Owen, P. Safa, R. W. Tsien, Ca(V)1 and Ca(V)2 channels engage distinct modes of Ca^{2+} signaling to control CREB-dependent gene expression. *Cell* **149**, 1112–1124 (2012).
9. R. E. Dolmetsch, U. Pajvani, K. Fife, J. M. Spotts, M. E. Greenberg, Signaling to the nucleus by an L-type calcium channel-calmodulin complex through the MAP kinase pathway. *Science* **294**, 333–339 (2001).
10. A. E. West, W. G. Chen, M. B. Dalva, R. E. Dolmetsch, J. M. Kornhauser, A. J. Shaywitz, M. A. Takasu, X. Tao, M. E. Greenberg, Calcium regulation of neuronal gene expression. *Proc. Natl. Acad. Sci. U.S.A.* **98**, 11024–11031 (2001).
11. V. Schulla, E. Renstrom, R. Feil, S. Feil, I. Franklin, A. Gjinovci, X. J. Jing, D. Laux, I. Lundquist, M. A. Magnuson, S. Obermuller, C. S. Olofsson, A. Salehi, A. Wendt, N. Klugbauer, C. B. Wollheim, P. Rorsman, F. Hofmann, Impaired insulin secretion and glucose tolerance in β cell-selective $Ca_v1.2$ Ca^{2+} channel null mice. *EMBO J.* **22**, 3844–3854 (2003).
12. A. Marcantoni, D. H. Vandael, S. Mahapatra, V. Carabelli, M. J. Sinnegger-Brauns, J. Striessnig, E. Carbone, Loss of Cav1.3 channels reveals the critical role of L-type and BK channel coupling in pacemaking mouse adrenal chromaffin cells. *J. Neurosci.* **30**, 491–504 (2010).
13. D. C. Hill-Eubanks, M. E. Werner, T. J. Heppner, M. T. Nelson, Calcium signaling in smooth muscle. *Cold Spring Harb. Perspect. Biol.* **3**, a004549 (2011).
14. A. Brandt, J. Striessnig, T. Moser, CaV1.3 channels are essential for development and presynaptic activity of cochlear inner hair cells. *J. Neurosci.* **23**, 10832–10840 (2003).
15. G. S. Pitt, M. Matsui, C. Cao, Voltage-gated calcium channels in nonexcitable tissues. *Annu. Rev. Physiol.* **83**, 183–203 (2021).
16. I. Splawski, K. W. Timothy, L. M. Sharpe, N. Decher, P. Kumar, R. Bloise, C. Napolitano, P. J. Schwartz, R. M. Joseph, K. Condouris, H. Tager-Flusberg, S. G. Priori, M. C. Sanguinetti, M. T. Keating, Ca(V)1.2 calcium channel dysfunction causes a multisystem disorder including arrhythmia and autism. *Cell* **119**, 19–31 (2004).
17. D. Endres, N. Decher, I. Rohr, K. Vowinkel, K. Domschke, K. Komlosi, A. Tzschach, B. Glaser, M. A. Schiele, K. Runge, P. Suss, F. Schuchardt, K. Nickel, B. Stallmeyer, S. Rinne, E. Schulze-Bahr, L. Tebartz van Elst, New Cav1.2 channelopathy with high-functioning autism, affective disorder, severe dental enamel defects, a short qt interval, and a novel cacna1c loss-of-function mutation. *Int. J. Mol. Sci.* **21**, 8611 (2020).
18. C. Antzelevitch, G. D. Pollevick, J. M. Cordeiro, O. Casis, M. C. Sanguinetti, Y. Aizawa, A. Guerchicoff, R. Pfeiffer, A. Oliva, B. Wollnik, P. Gelber, E. P. Bonaros Jr., E. Burashnikov, Y. Wu, J. D. Sargent, S. Schickel, R. Oberheiden, A. Bhatia, L. F. Hsu, M. Haissaguerre, R. Schimpf, M. Borggrefe, C. Wolpert, Loss-of-function mutations in the cardiac calcium channel underlie a new clinical entity characterized by ST-segment elevation, short QT intervals, and sudden cardiac death. *Circulation* **115**, 442–449 (2007).
19. L. H. Rodan, R. C. Spillmann, H. T. Kurata, S. M. Lamothe, J. Maghera, R. A. Jamra, A. Alkelai, S. E. Antonarakis, I. Atallah, O. Bar-Yosef, F. Bilan, K. Bjorgo, X. Blanc, P. Van Bogaert, Y. Bolkier, L. C. Burrage, B. U. Christ, J. L. Granadillo, P. Dickson, K. A. Donald, C. Dubourg, A. Eliyahu, L. Emrick, K. Engleman, M. V. Gonfiantini, J. M. Good, J. Kalser, C. Kloeckner, G. Lachmeijer, M. Macchiaiolo, F. Nicita, S. Odent, E. O'Heir, X. Ortiz-Gonzalez, M. Pacio-Miguez, M. Palomares-Bralo, L. Pena, K. Platzer, M. Quinodoz, E. Ranza, J. A. Rosenfeld, E. Roulet-Perez, A. Santani, F. Santos-Simarro, B. Pode-Shakked, C. Skraban, R. Slaugh, A. Superti-Furga, I. Thiffault, R. H. van Jaabrsveld, M. Vincent, H. G. Wang, P. Zacher, N. Undiagnosed Diseases, E. Rush, G. S. Pitt, P. Y. B. Au, V. Shashi, Phenotypic expansion of CACNA1C-associated disorders to include isolated neurological manifestations. *Genet. Med.* **23**, 1922–1932 (2021).
20. Z. D. Kabir, A. Martinez-Rivera, A. M. Rajadhyaksha, From gene to behavior: L-Type calcium channel mechanisms underlying neuropsychiatric symptoms. *Neurotherapeutics* **14**, 588–613 (2017).
21. S. Heyes, W. S. Pratt, E. Rees, S. Dahimene, L. Ferron, M. J. Owen, A. C. Dolphin, Genetic disruption of voltage-gated calcium channels in psychiatric and neurological disorders. *Prog. Neurobiol.* **134**, 36–54 (2015).
22. International Schizophrenia Consortium, S. M. Purcell, N. R. Wray, J. L. Stone, P. M. Visscher, M. C. O'Donovan, P. F. Sullivan, P. Sklar, Common polygenic variation contributes to risk of schizophrenia and bipolar disorder. *Nature* **460**, 748–752 (2009).
23. Cross-Disorder Group of the Psychiatric Genomics Consortium, Identification of risk loci with shared effects on five major psychiatric disorders: A genome-wide analysis. *Lancet* **381**, 1371–1379 (2013).
24. S. A. Ament, S. Szelinger, G. Glusman, J. Ashworth, L. Hou, N. Akula, T. Shekhtman, J. A. Badner, M. E. Brunkow, D. E. Mauldin, A. B. Stittrich, K. Rouleau, S. D. Detera-Wadleigh, J. I. Nurnberger Jr., H. J. Edenberg, E. S. Gershon, N. Schork, S. Bipolar Genome, N. D. Price, R. Gelinas, L. Hood, D. Craig, F. J. McMahon, J. R. Kelsoe, J. C. Roach, Rare variants in

neuronal excitability genes influence risk for bipolar disorder. *Proc. Natl. Acad. Sci. U.S.A.* **112**, 3576–3581 (2015).
25. A. Pinggera, J. Striessnig, Ca_v 1.3 (CACNA1D) L-type Ca^{2+} channel dysfunction in CNS disorders. *J. Physiol.* **594**, 5839–5849 (2016).
26. G. H. Hockerman, B. Z. Peterson, B. D. Johnson, W. A. Catterall, Molecular determinants of drug binding and action on L-type calcium channels. *Annu. Rev. Pharmacol. Toxicol.* **37**, 361–396 (1997).
27. T. Yang, Y. Suhail, S. Dalton, T. Kernan, H. M. Colecraft, Genetically encoded molecules for inducibly inactivating CaV channels. *Nat. Chem. Biol.* **3**, 795–804 (2007).
28. S. A. Kanner, T. Morgenstern, H. M. Colecraft, Sculpting ion channel functional expression with engineered ubiquitin ligases. *eLife* **6**, e29744 (2017).
29. A. Bourson, P. C. Moser, A. J. Gower, A. K. Mir, Central and peripheral effects of the dihydropyridine calcium channel activator BAY K 8644 in the rat. *Eur. J. Pharmacol.* **160**, 339–347 (1989).
30. R. C. Shelton, J. A. Grebb, W. J. Freed, Induction of seizures in mice by intracerebroventricular administration of the calcium channel agonist BAY k 8644. *Brain Res.* **402**, 399–402 (1987).
31. H. A. Jinnah, S. Yitta, T. Drew, B. S. Kim, J. E. Visser, J. D. Rothstein, Calcium channel activation and self-biting in mice. *Proc. Natl. Acad. Sci. U.S.A.* **96**, 15228–15232 (1999).
32. H. Chen, D. H. Vandorpe, X. Xie, S. L. Alper, M. L. Zeidel, W. Yu, Disruption of Cav1.2-mediated signaling is a pathway for ketamine-induced pathology. *Nat. Commun.* **11**, 4328 (2020).
33. W. A. Catterall, M. J. Lenaeus, T. M. Gamal El-Din, Structure and pharmacology of voltage-gated sodium and calcium channels. *Annu. Rev. Pharmacol. Toxicol.* **60**, 133–154 (2020).
34. G. Liu, A. Papa, A. N. Katchman, S. I. Zakharov, D. Roybal, J. A. Hennessey, J. Kushner, L. Yang, B. X. Chen, A. Kushnir, K. Dangas, S. P. Gygi, G. S. Pitt, H. M. Colecraft, M. Ben-Johny, M. Kalocsay, S. O. Marx, Mechanism of adrenergic CaV1.2 stimulation revealed by proximity proteomics. *Nature* **577**, 695–700 (2020).
35. M. Ben-Johny, D. T. Yue, Calmodulin regulation (calmodulation) of voltage-gated calcium channels. *J. Gen. Physiol.* **143**, 679–692 (2014).
36. M. T. Woon, P. A. Long, L. Reilly, J. M. Evans, A. M. Keefe, M. R. Lea, C. J. Beglinger, R. C. Balijepalli, Y. Lee, T. M. Olson, T. J. Kamp, Pediatric dilated cardiomyopathy-associated LRRC10 (leucine-rich repeat-containing 10) variant reveals LRRC10 as an auxiliary subunit of cardiac L-Type Ca^{2+} channels. *J. Am. Heart Assoc.* **7**, e006428 (2018).
37. N. L. Manuylov, E. Manuylova, V. Avdoshina, S. Tevosian, Serdin1/Lrrc10 is dispensable for mouse development. *Genesis* **46**, 441–446 (2008).
38. P. D. Nguyen, I. Gooijers, G. Campostrini, A. O. Verkerk, H. Honkoop, M. Bouwman, D. E. M. de Bakker, T. Koopmans, A. Vink, G. E. M. Lamers, A. Shakked, J. Mars, A. A. Mulder, S. Chocron, K. Bartscherer, E. Tzahor, C. L. Mummery, T. P. de Boer, M. Bellin, J. Bakkers, Interplay between calcium and sarcomeres directs cardiomyocyte maturation during regeneration. *Science* **380**, 758–764 (2023).
39. W. T. Stockdale, M. E. Lemieux, A. C. Killen, J. Zhao, Z. Hu, J. Riepsaame, N. Hamilton, T. Kudoh, P. R. Riley, R. van Aerle, Y. Yamamoto, M. T. M. Mommersteeg, Heart regeneration in the mexican cavefish. *Cell Rep.* **25**, 1997–2007.e7 (2018).
40. K. H. Kim, D. S. Antkiewicz, L. Yan, K. W. Eliceiri, W. Heideman, R. E. Peterson, Y. Lee, Lrrc10 is required for early heart development and function in zebrafish. *Dev. Biol.* **308**, 494–506 (2007).
41. R. J. Salamon, M. C. McKeon, J. Bae, X. Zhang, W. G. Paltzer, K. N. Wanless, A. R. Schuett, D. J. Nuttall, S. A. Nemr, R. Sridharan, Y. Lee, T. J. Kamp, A. I. Mahmoud, LRRC10 regulates mammalian cardiomyocyte cell cycle during heart regeneration. *NPJ Regen. Med.* **8**, 39 (2023).
42. M. J. Brody, L. Feng, A. C. Grimes, T. A. Hacker, T. M. Olson, T. J. Kamp, R. C. Balijepalli, Y. Lee, LRRC10 is required to maintain cardiac function in response to pressure overload. *Am. J. Physiol. Heart Circ. Physiol.* **310**, H269–H278 (2016).
43. P. Enkhbayar, M. Kamiya, M. Osaki, T. Matsumoto, N. Matsushima, Structural principles of leucine-rich repeat (LRR) proteins. *Proteins* **54**, 394–403 (2004).
44. N. Matsushima, S. Takatsuka, H. Miyashita, R. H. Kretsinger, Leucine rich repeat proteins: sequences, mutations, structures and diseases. *Protein Pept. Lett.* **26**, 108–131 (2019).
45. T. J. Morgenstern, J. Park, Q. R. Fan, H. M. Colecraft, A potent voltage-gated calcium channel inhibitor engineered from a nanobody targeted to auxiliary $Ca_V\beta$ subunits. *eLife* **8**, e49253 (2019).
46. Z. Buraei, J. Yang, The β subunit of voltage-gated Ca^{2+} channels. *Physiol. Rev.* **90**, 1461–1506 (2010).
47. E. Perez-Reyes, Molecular physiology of low-voltage-activated t-type calcium channels. *Physiol. Rev.* **83**, 117–161 (2003).
48. T. Yang, X. Xu, T. Kernan, V. Wu, H. M. Colecraft, Rem, a member of the RGK GTPases, inhibits recombinant CaV1.2 channels using multiple mechanisms that require distinct conformations of the GTPase. *J. Physiol.* **588**, 1665–1681 (2010).
49. B. Li, M. R. Tadross, R. W. Tsien, Sequential ionic and conformational signaling by calcium channels drives neuronal gene expression. *Science* **351**, 863–867 (2016).
50. D. G. Wheeler, C. F. Barrett, R. D. Groth, P. Safa, R. W. Tsien, CaMKII locally encodes L-type channel activity to signal to nuclear CREB in excitation-transcription coupling. *J. Cell Biol.* **183**, 849–863 (2008).
51. J. P. K. Ip, N. Mellios, M. Sur, Rett syndrome: Insights into genetic, molecular and circuit mechanisms. *Nat. Rev. Neurosci.* **19**, 368–382 (2018).
52. W. G. Chen, Q. Chang, Y. Lin, A. Meissner, A. E. West, E. C. Griffith, R. Jaenisch, M. E. Greenberg, Derepression of BDNF transcription involves calcium-dependent phosphorylation of MeCP2. *Science* **302**, 885–889 (2003).
53. Z. Zhou, E. J. Hong, S. Cohen, W. N. Zhao, H. Y. Ho, L. Schmidt, W. G. Chen, Y. Lin, E. Savner, E. C. Griffith, L. Hu, J. A. Steen, C. J. Weitz, M. E. Greenberg, Brain-specific phosphorylation of MeCP2 regulates activity-dependent Bdnf transcription, dendritic growth, and spine maturation. *Neuron* **52**, 255–269 (2006).
54. N. Ballas, D. T. Lioy, C. Grunseich, G. Mandel, Non-cell autonomous influence of MeCP2-deficient glia on neuronal dendritic morphology. *Nat. Neurosci.* **12**, 311–317 (2009).
55. Y. Li, H. Wang, J. Muffat, A. W. Cheng, D. A. Orlando, J. Loven, S. M. Kwok, D. A. Feldman, H. S. Bateup, Q. Gao, D. Hockemeyer, M. Mitalipova, C. A. Lewis, M. G. Vander Heiden, M. Sur, R. A. Young, R. Jaenisch, Global transcriptional and translational repression in human-embryonic-stem-cell-derived Rett syndrome neurons. *Cell Stem Cell* **13**, 446–458 (2013).
56. M. Chahrour, S. Y. Jung, C. Shaw, X. Zhou, S. T. Wong, J. Qin, H. Y. Zoghbi, MeCP2, a key contributor to neurological disease, activates and represses transcription. *Science* **320**, 1224–1229 (2008).
57. Y. Liu, A. Flamier, G. W. Bell, A. J. Diao, T. W. Whitfield, H. C. Wang, Y. Wu, F. Schulte, M. Friesen, R. Guo, M. Mitalipova, X. S. Liu, S. M. Vos, R. A. Young, R. Jaenisch, MECP2 directly interacts with RNA polymerase II to modulate transcription in human neurons. *Neuron* **112**, 1943–1958.e10 (2024).
58. J. Qian, X. Guan, B. Xie, C. Xu, J. Niu, X. Tang, C. H. Li, H. M. Colecraft, R. Jaenisch, X. S. Liu, Multiplex epigenome editing of *MECP2* to rescue Rett syndrome neurons. *Sci. Transl. Med.* **15**, eadd4666 (2023).
59. W. Yu, Reviving Cav1.2 as an attractive drug target to treat bladder dysfunction. *FASEB J.* **36**, e22118 (2022).
60. I. F. Khan, R. K. Hirata, D. W. Russell, AAV-mediated gene targeting methods for human cells. *Nat. Protoc.* **6**, 482–501 (2011).
61. Q. Bu, A. Wang, H. Hamzah, A. Waldman, K. Jiang, Q. Dong, R. Li, J. Kim, D. Turner, Q. Chang, CREB signaling is involved in Rett syndrome pathogenesis. *J. Neurosci.* **37**, 3671–3685 (2017).
62. A. Banerjee, R. V. Rikhye, V. Breton-Provencher, X. Tang, C. Li, K. Li, C. A. Runyan, Z. Fu, R. Jaenisch, M. Sur, Jointly reduced inhibition and excitation underlies circuit-wide changes in cortical processing in Rett syndrome. *Proc. Natl. Acad. Sci. U.S.A.* **113**, E7287–E7296 (2016).
63. R. C. Samaco, J. L. Neul, Complexities of Rett syndrome and MeCP2. *J. Neurosci.* **31**, 7951–7959 (2011).
64. Q. Dong, Q. Liu, R. Li, A. Wang, Q. Bu, K. H. Wang, Q. Chang, Mechanism and consequence of abnormal calcium homeostasis in Rett syndrome astrocytes. *eLife* **7**, e33417 (2018).
65. S. Kamijo, Y. Ishii, S. I. Horigane, K. Suzuki, M. Ohkura, J. Nakai, H. Fujii, S. Takemoto-Kimura, H. Bito, A critical neurodevelopmental role for L-type voltage-gated calcium channels in neurite extension and radial migration. *J. Neurosci.* **38**, 5551–5566 (2018).
66. J. N. Muth, I. Bodi, W. Lewis, G. Varadi, A. Schwartz, A Ca^{2+}-dependent transgenic model of cardiac hypertrophy: A role for protein kinase Cα. *Circulation* **103**, 140–147 (2001).
67. B. M. Ahern, B. M. Levitan, S. Veeranki, M. Shah, N. Ali, A. Sebastian, W. Su, M. C. Gong, J. Li, J. E. Stelzer, D. A. Andres, J. Satin, Myocardial-restricted ablation of the GTPase RAD results in a pro-adaptive heart response in mice. *J. Biol. Chem.* **294**, 10913–10927 (2019).
68. M. J. Brody, Y. Lee, The role of leucine-rich repeat containing protein 10 (LRRC10) in dilated cardiomyopathy. *Front. Physiol.* **7**, 337 (2016).
69. M. J. Brody, T. A. Hacker, J. R. Patel, L. Feng, J. Sadoshima, S. G. Tevosian, R. C. Balijepalli, R. L. Moss, Y. Lee, Ablation of the cardiac-specific gene leucine-rich repeat containing 10 (Lrrc10) results in dilated cardiomyopathy. *PLOS ONE* **7**, e51621 (2012).
70. X. K. Qu, F. Yuan, R. G. Li, L. Xu, W. F. Jing, H. Liu, Y. J. Xu, M. Zhang, X. Liu, W. Y. Fang, Y. Q. Yang, X. B. Qiu, Prevalence and spectrum of LRRC10 mutations associated with idiopathic dilated cardiomyopathy. *Mol. Med. Rep.* **12**, 3718–3724 (2015).
71. L. Huang, S. Tang, Y. Chen, L. Zhang, K. Yin, Y. Wu, J. Zheng, Q. Wu, J. C. Makielski, J. Cheng, Molecular pathological study on LRRC10 in sudden unexplained nocturnal death syndrome in the Chinese Han population. *Int. J. Leg. Med.* **131**, 621–628 (2017).
72. P. J. Adams, M. Ben-Johny, I. E. Dick, T. Inoue, D. T. Yue, Apocalmodulin itself promotes ion channel opening and Ca^{2+} regulation. *Cell* **159**, 608–622 (2014).
73. J. Niu, I. E. Dick, W. Yang, M. A. Bamgboye, D. T. Yue, G. Tomaselli, T. Inoue, M. Ben-Johny, Allosteric regulators selectively prevent Ca^{2+}-feedback of Ca_V and Na_V channels. *eLife* **7**, e35222 (2018).
74. B. Z. Stanton, E. J. Chory, G. R. Crabtree, Chemically induced proximity in biology and medicine. *Science* **359**, eaao5902 (2018).

75. J. Niu, M. Ben Johny, I. E. Dick, T. Inoue, Following Optogenetic dimerizers and quantitative prospects. *Biophys. J.* **111**, 1132–1140 (2016).
76. G. G. Gross, J. A. Junge, R. J. Mora, H. B. Kwon, C. A. Olson, T. T. Takahashi, E. R. Liman, G. C. Ellis-Davies, A. W. McGee, B. L. Sabatini, R. W. Roberts, D. B. Arnold, Recombinant probes for visualizing endogenous synaptic proteins in living neurons. *Neuron* **78**, 971–985 (2013).
77. N. Chakouri, S. Rivas, D. Roybal, L. Yang, J. Diaz, A. Hsu, R. Mahling, B. X. Chen, J. O. Owoyemi, D. DiSilvestre, D. Sirabella, B. Corneo, G. F. Tomaselli, I. E. Dick, S. O. Marx, M. Ben-Johny, Fibroblast growth factor homologous factors serve as a molecular rheostat in tuning arrhythmogenic cardiac late sodium current. *Nat. Cardiovasc. Res.* **1**, 1–13 (2022).
78. J. Abramson, J. Adler, J. Dunger, R. Evans, T. Green, A. Pritzel, O. Ronneberger, L. Willmore, A. J. Ballard, J. Bambrick, S. W. Bodenstein, D. A. Evans, C. C. Hung, M. O'Neill, D. Reiman, K. Tunyasuvunakool, Z. Wu, A. Zemgulyte, E. Arvaniti, C. Beattie, O. Bertolli, A. Bridgland, A. Cherepanov, M. Congreve, A. I. Cowen-Rivers, A. Cowie, M. Figurnov, F. B. Fuchs, H. Gladman, R. Jain, Y. A. Khan, C. M. R. Low, K. Perlin, A. Potapenko, P. Savy, S. Singh, A. Stecula, A. Thillaisundaram, C. Tong, S. Yakneen, E. D. Zhong, M. Zielinski, A. Zidek, V. Bapst, P. Kohli, M. Jaderberg, D. Hassabis, J. M. Jumper, Accurate structure prediction of biomolecular interactions with AlphaFold 3. *Nature* **630**, 493–500 (2024).
79. K. Deisseroth, E. K. Heist, R. W. Tsien, Translocation of calmodulin to the nucleus supports CREB phosphorylation in hippocampal neurons. *Nature* **392**, 198–202 (1998).

Acknowledgments: We thank members of the Calcium Signals Laboratory–Columbia for valuable insight and feedback on this work. Research supported in this publication was performed in the Columbia CCTI Flow cytometry core, supported in part by the Office of the Director, National Institutes of Health, under the award S10RR027050. Images were collected and analyzed in the Confocal and Specialized Microscopy Shared Resource of the Herbert Irving Comprehensive Cancer Center at Columbia University, supported by National Institutes of Health (NIH) grant P30 CA013696 (National Cancer Institute). The content is solely the responsibility of the authors and does not necessarily represent the official views of the NIH. **Funding:** This study is supported by funding from NHLBI (P01 HL164319), NINDS (R01 NS110672), NIDA (R01DA053261), Austrian Science Fund (FWF 10.55776/P36053), and the American Heart Association (for P.J.d.R.M.). **Author Contributions:** Conceptualization: P.J.d.R.M., M.B.-J., and X.S.L. Methodology: H.M.C., A.L.K., D.S.C., L.Y., S.M.G., M.B.-J., P.J.d.R.M., X.S.L., S.J., and A.M.R. Software: M.B.-J. and S.J. Validation: H.M.C., A.L.K., P.T., L.Y., M.B.-J., P.J.d.R.M., S.J., and A.M.R. Formal analysis: A.L.K., P.T., D.S.C., M.B.-J., P.J.d.R.M., S.J., and A.M.R. Investigation: A.L.K., P.T., D.S.C., S.O.M., L.Y., S.M.G., M.B.-J., P.J.d.R.M., X.S.L., S.J., and A.M.R. Resources: H.M.C., A.L.K., P.T., S.O.M., L.Y., M.B.-J., P.J.d.R.M., X.S.L., and S.J. Writing—original draft: D.S.C., M.B.-J., P.J.d.R.M., and S.J. Writing—review and editing: H.M.C., A.L.K., P.T., S.O.M., L.Y., M.B.-J., P.J.d.R.M., S.J., and A.M.R. Visualization: P.T., D.S.C., L.Y., M.B.-J., P.J.d.R.M., S.J., and A.M.R. Supervision: H.M.C., P.T., S.O.M., M.B.-J., and A.M.R. Funding acquisition: P.T., S.O.M., M.B.-J., P.J.d.R.M. Project administration: P.T., S.O.M., M.B.-J., and X.S.L. Data curation: L.Y., M.B.-J., and S.J. **Competing Interests:** P.J.d.R.M. and M.B.-J. are inventors on a provisional patent submitted by Columbia University for GeeC_L (44010.180WO-PCT) filed on 30 June 2023. XSL is a cofounder for Epitor Therapeutics. The other authors declare that they have no competing interests. **Data and materials availability:** All data needed to evaluate the conclusions in the paper are present in the paper and/or the Supplementary Materials.

Submitted 9 May 2024
Accepted 24 September 2024
Published 30 October 2024
10.1126/sciadv.adq3374